



MINISTRY OF TECHNOLOGY

AERONAUTICAL RESEARCH COUNCIL
REPORTS AND MEMORANDA

Notes on the Progress of Free-Flight Trials to
Measure Heat Transfer at Mach Numbers up
to 5

By J. PICKEN, B.Sc. and R. HARMER

LIBRARY
ROYAL AIR FORCE ESTABLISHMENT
WINDSOR

LONDON: HER MAJESTY'S STATIONERY OFFICE

1967

PRICE £1 5s. 6d. NET

Notes on the Progress of Free-Flight Trials to Measure Heat Transfer at Mach Numbers up to 5

By J. PICKEN, B.Sc. and R. HARMER

COMMUNICATED BY THE DEPUTY CONTROLLER AIRCRAFT (RESEARCH AND DEVELOPMENT),
MINISTRY OF AVIATION

*Reports and Memoranda No. 3432**
June, 1958

Summary.

A summary of the first ten flights made with a heat-transfer vehicle is given together with some of the salient features of the results relative to conical and hemispherical heads. The method of reducing the temperature data is outlined.

The turbulent heating rates to a cone were overestimated by about 12% on the average by a theory^{1,11} based on 'intermediate' enthalpy, a Reynolds analogy factor of 1.22 and a cone form factor of 1.18.

The data relative to hemispherical heads indicate the following results.

(i) Fair agreement is obtained with the theory of Stine and Wanlass² at the stagnation point and some agreement at those stations identified with laminar flow.

(ii) On the whole predictions for turbulent heat transfer on the basis of Peattie and Wild³ are closer than those on the basis of Van Driest⁴ but neither give a satisfactory correlation of all the data.

(iii) The roughness of the surface finish can give rise to an appreciable increase in turbulent heat-transfer rate. A 10 inch diameter hemisphere with a C.L.A. finish of 200 microinches was found to have turbulent heat-transfer rates about 30% greater on the average than those of a similar smooth one.

(iv) The distance of the boundary between laminar and turbulent flow from the nose was not the same along different streamlines radiating from the stagnation point.

Further experiments planned are briefly described.

LIST OF CONTENTS

Section

1. Introduction
2. Description of Test Vehicle
 - 2.1 Test body
 - 2.2 Heat-transfer heads
 - 2.3 Instrumentation

*Replaces R.A.E. Tech. Note No. Aero. 2575—A.R.C. 20 802.

LIST OF CONTENTS—*continued*

3. Vehicles Flown
 - 3.1 Rocket motor failures
 - 3.2 Telemetry failures
4. Data Reduction
5. Heat Transfer to Conical Head
 - 5.1 Theoretical background
 - 5.2 Results and discussion
 - 5.2.1 Reynolds analogy factor
6. Heat Transfer to Hemispheres
 - 6.1 Local flow conditions
 - 6.2 Theoretical predictions
 - 6.3 Results
7. Conclusions
 - 7.1 Cone
 - 7.2 Hemispheres

List of Symbols

References

Tables 1 to 4c

Illustrations—Figs. 1 to 30

Detachable Abstract Cards

LIST OF TABLES

Table

1. Physical data for vehicle
2. Summary of flights made between 9.2.56 and 9.7.57
3. Location of stations, local wall thickness and flow regime for heads 3, 5, 6 and 8
4. Predicted and experimental values of Stanton number, k_H , vs. location of station and free-stream Mach number for heads 5, 6 and 8

LIST OF ILLUSTRATIONS

Figure

1. Sketch of test vehicles
2. Fin assembly
3. Head and instrumentation assembly

LIST OF ILLUSTRATIONS—*continued*

Figure

4. Details of junctions of instrument compartment with the head and rocket motor
5. Assembled vehicle prepared for flight
6. Talysurf records of surface profiles
7. Thermocouple weld
8. Internal view of head showing location of thermocouples
9. Insulating Durestos covers on 10 inch hemispheres (heads 5 and 6)
10. Durestos inner wall
11. Flares attached to fin assembly
12. Block diagram of telemetry equipment
13. Telemetry unit
14. Variation of heat capacity per unit area with temperature for mild steel
15. Typical telemetry record
16. System of head co-ordinates
17. Trajectory data for cone (head 3)
18. Trajectory data for hemispherical heads 5, 6, 8 and 9
19. Variation of wall temperature with time for hemispherical heads 5, 6, 8 and 9
20. Local heat-transfer rate histories for heads 3, 5, 6, 8 and 9
21. Variation of local Reynolds number, R , with time for the stations of hemispherical head 5
- 22a. Temperature histories of insulating air gap in 4 inch hemisphere (head 9)
- 22b. Temperature histories of air along axis of uninsulated 4 inch hemisphere (head 8)
23. Comparison of temperature measurements with theory for conical head 3
24. Comparison of experimental Stanton numbers with theory for conical head 3
25. Variation of Reynolds analogy factor with Reynolds number for cone for two reference enthalpies
26. Variation of N_w/\sqrt{R} at the stagnation point with time for hemispheres
27. Flow regimes on hemispherical heads
28. Variation of N_w/\sqrt{R} with free-stream Mach number at stations (30° , 0°) and (45° , 180°) on the 10 inch smooth hemisphere
29. Comparison of measured heat transfer rate with that predicted by Peattie and Wild³ for turbulent flow round hemispheres

}	Variation of mean value of ratio over Mach number range with angle
	Variation of mean value of ratio over angle range with Mach number
30. Comparison of Stanton numbers, k_H , corrected and uncorrected for wall conductivity at two stations on the 4 inch hemisphere (head 8)

1. Introduction.

In the U.K., existing ground facilities for heat-transfer experimentation do not provide combinations of Mach number, Reynolds number, total temperature and, except in the case of the shock tube, local-stream to wall-temperature ratio which are adequately high for the results to be applied directly to certain aircraft and missile projects. The combinations can, to some extent, be provided by free-flight facilities. The Free Flight Group of Aerodynamics Department at the Royal Aircraft Establishment have developed a vehicle for this purpose and up to the present, have flown ten at Aberporth at Mach numbers up to about 5. The vehicle has been evolved from Guided Weapons Department's C.T.V.5 series 2⁵ and consists essentially of a solid-fuel rocket motor with stabilising fins and a head of variable form.

This report outlines the present position regarding the experiments and the interpretation of the results so far analysed.

2. Description of Test Vehicle.

At the outset of these experiments the Royal Aircraft Establishment Rocket Propulsion Department was developing a solid-fuel rocket motor with an overall specific impulse markedly better than those of others then available. Its total impulse was estimated to be high enough to be of value for aerodynamic heating investigations without staging.

2.1. Test Body.

The test body consists of three major components namely the rocket motor, the fin assembly and the instrumentation compartment. Fig. 1 gives a sketch of the general arrangement. Fig. 2 shows the fin assembly. This is substantially the same as that used for the C.T.V.5 series 2⁵, except that mild-steel sheet was used in place of dural for the fin skin and the steel leading edges were radiused to reduce possible distortion through aerodynamic heating. Details of the components forward of the rocket motor and the junction with the latter are illustrated in Figs. 3 and 4. Fig. 5 shows a photograph of a vehicle assembled just prior to launch. Typically, the maximum diameter is 10½ inches, the overall length about 15 ft and the weight 650 lb to 700 lb. Physical data for a typical vehicle are given in Table 1.

2.2. Heat-Transfer Heads.

The heads so far flown are summarised in Table 2 and sketched in Fig. 1. Heads 1 to 4 and 10 were cones of 16° 40' inclusive angle, and heads 5 to 9 were hemisphere cylinders, 5 and 6 being 10 inches diameter and 7 to 9, 4 inches diameter. They were fabricated in steel sheet with the exception of head 10 which was machined from solid steel in an attempt to reduce local variations in thickness and profile to a minimum. Wall thicknesses for the heat-transfer heads varied from a mean value of 0.024 inches for conical head 3 to 0.066 inches for the 4 inch hemispherical head 9. With the fabricated method of construction the variation of local thickness was of the order of ±5%. We have not yet had sufficient experience with the machining method to assess its efficiency. In the case of head 10 the local thickness variation was not much better than would have been obtained with a fabricated head.

The external finish was attained by machine and hand polishing with fine-grade emery cloth except in the case of head 6 (10 inch hemisphere) which was roughened by sand blasting. The quality of the finish was assessed by a Talysurf⁶. This instrument produces a graph of the deviations of a sample of a surface from a smooth curve and computes the mean value of the deviations. This latter quantity is referred to as the centre line average or C.L.A. Most American workers quote the root-mean-square value for surface finish. The relationship between the latter and the C.L.A. depends on the details of the variation of the deviations. For a regular saw-toothed variation, the r.m.s. value = 1.15 C.L.A. and for a normal frequency distribution the r.m.s. value = 1.25 C.L.A. Some typical Talysurf records are reproduced in Fig. 6. As can be seen, there are occasional small areas of the smooth finishes where the roughness is gross compared with the average. C.L.A. values for smooth finishes were of the order of 4 microinches.

Wall temperature was sensed by thermocouples of Chromel and Alumel wire 0.005 inches in diameter. Each thermocouple was formed by arc welding two component wire ends together in a non-oxidising atmosphere of coal gas as described in Ref. 7. A ball of about 0.010 inches to 0.015 inches diameter was formed at the ends and this was then welded to the inner skin of the head at the station of interest by means of a miniature spot welder. The head itself was formed into one electrode through its periphery in order to avoid destroying the external surface finish locally. An enlarged photograph of a typical thermocouple attachment is given in Fig. 7 and of the inside of a head just after the installation of the thermocouples in Fig. 8. Each wire was electrically insulated by a sleeving of braided fibreglass. Details of the locations of the thermocouples on heads 3, 5, 6 and 8 are given in Table 3.

The air inside a head was thought to be the major potential medium of heat loss to the interior and it was considered desirable to restrict this function by impeding its convection and reducing its effective heat capacity. To this end, head 2 was stuffed with glass wool. However the packing pressures required to reduce the relative movement of the wool to safe proportions under rocket acceleration were so high that heat loss by conduction to the insulation material itself seemed likely to give rise to an additional complication and uncertainty⁸. Thus, in heads 3 to 6, Durestos discs or channels were placed over the thermocouple stations to restrict convection and limit the heat capacity of the air locally (Fig. 9). Fixing the discs and channels in position was awkward since temperature resistant cements such as Sirasil⁹ were ineffective on account of the rapidity of the heating, and it was found necessary to rivet them to the head wall, thus giving rise to a potential disturbance of the external finish. The method also added an element of asymmetry to the heat flux to the head. In heads 7, 9 and 10, these disadvantages were overcome by fitting a Durestos inner wall (Fig. 10). Between this and the outer wall, was an airgap of about 0.1 inches. In head 8, no attempt was made to restrict the convection or heat capacity of the internal air.

2.3. Instrumentation.

Free-stream velocity, static pressure and ambient temperature were measured by instruments external to the vehicle in accordance with the usual procedures at Aberporth. Reflection radio-Doppler and kiné-theodolites provided the most satisfactory means of measuring velocity. Initially some difficulty in tracking with kiné-theodolites was experienced but this has now been overcome by fitting flares (Fig. 11). Transponder radio-Doppler has also been tried but has not been successful owing to failure of the airborne components, probably as a result of the high longitudinal acceleration at launch.

The wall temperature at stations of interest was measured by telemetry equipment housed in the vehicle itself. This equipment is described in detail in Ref. 10. A block diagram outlining the salient features is given in Fig. 12 and a photograph of the physical arrangement in the vehicle in Fig. 13. The voltage output from the thermocouples is sampled by a two-pole scanning switch and then amplified about 100 times (by a transistorized A.C. amplifier) from a maximum of about 0.025 volts ($\equiv 650^{\circ}\text{C}$) to 2.5 volts. The amplified voltage is then transformed into a frequency in the 130 to 160 kc/s. band. This modulates a 465 Mc/s carrier wave which is transmitted from the vehicle to ground recording equipment.

The switch motor is driven at a speed of 80 c/s. It has 24 double contacts providing 24 channels of information each cycle. These are utilised as indicated in Fig. 12. A portion of a typical record is illustrated in Fig. 15. In a given cycle the first channel is used for the transmission of a synchronising pulse. Since the amplifier is of the A.C. type, the integral of the signals amplified should be approximately zero. It is thus convenient to transmit the thermocouple signals in pairs of opposite polarity and of about the same absolute magnitude, relative to some bias voltage injected after amplification. An earth or zero signal is transmitted just before and after each pair. On the record the distance between a deflection and its adjacent earth line provides a measure of the temperature sensed by the thermocouple (Fig. 15). Just prior to launch, a number of known voltages of positive and negative polarity are transmitted over the 3rd and 4th channels respectively, thus providing a calibration for the subsequent temperature deflections. During flight these same channels transmit a constant voltage again in a positive and negative sense respectively and this serves to monitor the pre-flight calibration. Thus in effect this arrangement

allows the transmission of temperature measurements from a maximum of 13 thermocouple stations about every 1/80 sec.

3. *Vehicles Flown.*

A summary of the flights made is given in Table 2, together with a brief description of their purpose and the duration of the useful records obtained. Flights 1 and 4 were made primarily to investigate the mechanical integrity of the vehicle. Flights 2 and 3 were designed to obtain heat transfer relative to the well established flow data for a slim cone in order that a comparison could be made with the results of other workers, and if possible with Eckert's intermediate enthalpy theory¹¹.

Hemisphere cylinders were flown in flights 5 to 9 in order to supplement the free-flight experiments made by Guided Weapons Department^{5,12}, and directed towards a specific project. The primary interest lay in the effects of high Reynolds number, and of roughness on transition and the turbulent heat-transfer rate.

Flight 10 was made with a slim conical head and was intended as the first of a series of four, to investigate roughness further.

Only in flight 9 were complete records obtained for the whole trajectory. Useful data in the other flights were largely limited to the acceleration period, primarily because of telemetry failures (four vehicles), failure of the kiné-theodolites to track the vehicle (three cases), destruction of the vehicle through the rocket motor exploding (one case) and failure to operate the ground recording equipment (one case).

3.1. *Rocket Motor Failures.*

In flights 1 to 4 the rocket motor exploded towards the end of the acceleration period or shortly after. This was not altogether unexpected since these constituted the first flight trials of the motor development programme. As a result of the experience, R.A.E., Westcott, were able to identify and remedy the defects in the motor design. In the subsequent six flights the vehicles remained intact throughout their trajectories.

3.2. *Telemetry Failures.*

The telemetry equipment failed to operate satisfactorily in flights 2, 3, 4 and 10. In flight 2 the symptoms were suggestive of a short circuit in the arrangement of thermocouple wires. In the other flights the failures were attributed to the effects of high longitudinal acceleration (typically 70g). In flights 3 and 4 the record became unintelligible. In flight 10 it was completely absent during the acceleration period, but became partially coherent for the remainder of the trajectory.

4. *Data Reduction.*

The objects of the data reduction operation were, firstly, to obtain from the telemetry record, histories of the outside skin temperature and of the heat flowing into the wall from the boundary layer at the stations of interest on a head, and secondly, to combine these quantities with the trajectory data and the geometry of the head to form the heat-transfer coefficients described in Sections 5 and 6.

In the estimation of heat input from the boundary layer it has been assumed that :

(i) Radiation effects are zero. Even at the maximum skin temperature of about 650°C, losses by radiation should not exceed 0.5 C.H.U./ft² and for the polished heads, should be substantially less than this.

(ii) Heat loss to the interior is zero. As yet we have made no direct measurements of heat flow from the inner skin to the interior. Although with the insulation precautions described above, it is likely to be for the most part relatively small, we cannot be certain that it is negligible. Further laboratory investigations are required before we can neglect it or estimate it with confidence.

(iii) The temperature gradient through the wall is zero. Where this assumption is doubtful, we can now make subsequent adjustments on an analogue computer. The results presented in the present report however, have not been so adjusted and the experimental heat-transfer coefficients quoted may be in error by a few per cent on this account, particularly in the region of maximum velocity for the

hemispheres. No significant adjustment should be required for the thinner-walled conical head 3. The adjustments required for the hemispherical stations should not exceed that illustrated in Fig. 30 for station (50°, 0°) on the 4 inch hemispherical head 8.

These assumptions allow us to equate the local heat flow rate per unit area from the boundary layer to the head with the heat absorbed by the wall of the latter in unit time per unit area, in the form:

$$q = G \frac{dT_w}{dt} \quad (1)$$

where

T_w is the wall temperature

$G = \delta \tau \sigma$ is the heat capacity of the wall per unit area

δ = the density of the wall

τ = the thickness of the wall

σ = the specific heat of the wall.

The values of δ and σ used were those for mild steel given in Ref. 13. Fig. 14 shows how the ratio of heat capacity per unit area to the wall thickness at 15°C varies with temperature.

Now the accuracy of the temperature measurements was of the order of $\pm 1\%$ to $\pm 3\%$ of full scale and presented the greatest source of inaccuracy in the calculation of $d T_w/dt$ and hence of the heat transfer rate. The need for some efficient averaging technique was soon apparent and in the first instance (up to flight 6) Spencer's 21-point formula¹⁴ was used* for smoothing and the first derivative was obtained by three point differentiation of the smoothed values.

For the acceleration parts of flights 8 and 9 we applied* 21-point least-squares formulae¹⁵ for smoothing and differentiating, using a high-speed digital computer (DEUCE). A cubic was selected arbitrarily because this seemed to be the lowest degree of polynomial that would allow efficient smoothing without destroying the significant irregularities caused by boundary-layer transition and variation of wall heat capacity. However, the derivatives obtained by this process showed appreciable scatter and consideration is now being given to the development of an optimized procedure along the lines suggested by Ref. 16.

5. Heat Transfer to a Conical Head.

5.1. Theoretical Background.

Head 3 was the only conical head from which heat-transfer data were extracted. Ref. 17 gives a preliminary description of the results obtained and of the relevance of these to variants of the intermediate-enthalpy formula proposed by Eckert¹¹ and recommended by Monaghan¹ for estimating heat-transfer rates from a turbulent boundary layer.

These formulae have been devised for estimating skin friction or heat transfer in compressible flow with either a laminar or turbulent boundary layer. In essence a standard formula for incompressible flow is applied to compressible flow by evaluating density and viscosity at an 'Intermediate Enthalpy' (or temperature) which is defined by an equation involving Mach number, surface temperature and ambient temperature.

Eckert's formula for intermediate enthalpy (h^*) is

$$h^* = h_1 + 0.5 (h_w - h_1) + 0.22 (h_{w0} - h_1) \quad (2)$$

*The temperature data were split into two interlacing sets which were separately processed and used in the subsequent analysis. Both sets of results are included in the plots presented for the reduced data. The differences between them gives a measure of reading inaccuracy.

where suffices 1, w and wo refer to conditions in the stream outside the boundary layer, at the wall, and at the wall under zero-heat-transfer conditions respectively. This we shall call 'formula b'.

Earlier work at the R.A.E. (see review in Ref. 18) had suggested that the turbulent-heat-transfer coefficient was a function only of wall temperature and not of Mach number. This can be fitted into the framework of equation (2) by defining

$$h^* = h_1 + 0.72 (h_w - h_1) \quad (3)$$

This we shall call 'formula a'.

Finally, there is the possibility that the turbulent-heat-transfer coefficient is a function of Mach number, but not of surface temperature. This would give

$$h^* = h_1 + 0.72 (h_{wo} - h_1) \quad (4)$$

which we shall call 'formula c'.

The zero heat-transfer enthalpy, h_{wo} , is related to local enthalpy and Mach number by the equation:

$$\frac{h_{wo}}{h_1} = 1 + r \frac{\gamma - 1}{2} M_1^2 \quad (5)$$

where r is the *enthalpy recovery factor*.

For the theoretical estimates in Section 5.2, a value of $r = 0.88$ was assumed on the basis of a discussion given in Ref. 1.

The rate of heat transfer from the boundary layer to the wall can be expressed as¹

$$q = k_H \rho_1 u_1 (h_{wo} - h_w) \quad (6)$$

where k_H is the non-dimensional heat-transfer coefficient (*Stanton number*)

$$\left. \begin{array}{l} \rho_1 \text{ is the density} \\ u_1 \text{ is the velocity} \end{array} \right\} \text{ of the air just outside the boundary layer.}$$

Alternatively we can refer the Stanton number to the density at the reference enthalpy and write equation (6) in the equivalent form

$$q = k_H^* \rho^* u_1 (h_{wo} - h_w) \quad (7)$$

whence we note

$$k_H = \frac{\rho^*}{\rho} k_H^* \quad (8)$$

Now heat-transfer is related to skin friction by the *Reynolds analogy factor*,

$$s = \frac{k_H}{\frac{1}{2} C_f}$$

For incompressible flow over a flat plate, using a formula of the Prandtl-Schlichting type for local turbulent skin friction, namely

$$C_{f_i} = 0.288 (\log_{10} R)^{-2.45} \quad (9)$$

we obtain

$$k_{H_i} = 0.144 s(\log_{10} R)^{-2.45} \quad (10)$$

where the suffix *i* refers quantities to incompressible flow conditions. For compressible flow, the same procedure is applied with regard to the reference enthalpy. Thus a compressible flow heat-transfer coefficient is given by

$$k_{H^*} = 0.144 s(\log_{10} R^*)^{-2.45} \quad (11)$$

and, from equation (7), when referred to conditions just outside the boundary layer this becomes.

$$k_H = 0.144 s \frac{\rho^*}{\rho_1} \left(\log_{10} R \frac{\rho^*}{\rho_1} \frac{\mu_1}{\mu^*} \right)^{-2.45} \quad (12)$$

Alternatively we may write it in the form

$$s = \frac{k_H}{0.144} \frac{\rho_1}{\rho^*} \left(\log_{10} R \frac{\rho^*}{\rho_1} \frac{\mu_1}{\mu^*} \right)^{-2.45} \quad (13)$$

In a review⁶ Seiff obtains a mean value of 1.22 for the Reynolds analogy factor, *s*, and detects no consistent variations with *M* or *T_w/T₁*. There is, however, a suggestion of some variation with Reynolds number.

For heat transfer to a cone, local values of enthalpy and Mach number outside the boundary layer must be used when evaluating *h** from equations (2) to (4); *u*₁ is the local velocity, and the value of *k_H* from equation (12) must be multiplied by a factor *f*, which we shall call a *form factor*, to allow for conical as distinct from flat-plate conditions. Refs. 19 and 20 suggest that for turbulent flow about a cone the value of *f* should be of the order of 1.15 to 1.20. On the other hand Buglia in Ref. 21 claims better agreement with experiment for a form factor of 1 for a blunt cone.

The majority of existing experimental data are for conditions fairly close to zero heat transfer where there is little difference between formulae a, b and c. So there is interest in results with the large rates of heat-transfer which a free-flight vehicle can provide.

5.2. Results and Discussion.

Figs. 23 and 24, show the results from head 3 for seven stations on the cone, between two and three seconds after launching, and compare them with the predictions of formulae a, b and c in conjunction with equation (12) assuming a constant form factor of 1.18 and a constant Reynolds analogy factor of 1.22. Fig. 23 is a plot of temperature and Fig. 24 of Stanton number, *k_H*, against time of flight and an auxiliary Mach number scale. Relevant trajectory data are presented in Fig. 17. Local flow conditions were obtained from these and Ref. 22.

In both Figs. 23 and 24, the experimental results lie mainly between the predictions of formulae 'b' and 'c' but do not agree with formula 'a'. The results of some N.A.C.A. flight tests (e.g. Refs. 23 to 25) when analysed in the same way, show a similar trend.

A comparison of the temperatures recorded at various stations along the cone, indicates that the derived heat-transfer rates should not have been affected significantly by temperature gradients in a longitudinal direction. On the other hand there would be heat loss to the air inside the head, and this could have the effect of reducing the apparent aerodynamic heat-transfer rates. This heat loss is difficult to calculate and it may not have been negligible. Therefore, at this stage it would not be wise to assume 'formula b' is inferior to 'formula c'. Methods of satisfactorily insulating the inner skin from, and estimating the heat loss to, the interior of the head are under investigation.

5.2.1. *Reynolds analogy factor and form factor.* Seiff's review²⁵ suggests that the Reynolds analogy factor ($s = k / \frac{1}{2} C_f$) may be a function of Reynolds number. Experimental values of Reynolds analogy factor were evaluated by substituting in equation (13) the experimental values of kH , obtained from the measurements and equation (6), divided by the form factor of 1.18 to allow for conical flow. In Fig. 25a, this ratio is plotted against Reynolds number with the reference enthalpy corresponding to 'formula c' for all stations, and in Fig. 25b a similar plot is given for intermediate enthalpy (formula b). In both figures, Seiff's mean value of 1.22 and the trend he found with Reynolds number, are also shown. For a correct reference enthalpy, the plots for the various stations might be expected to collapse onto a common curve. The accuracy of the processed data does not appear to be sufficient to detect this, whilst the general trend either favours a constant value, or is in the opposite direction to that suggested by Seiff. The values using intermediate enthalpy seem on the whole closer to those of Seiff than do the others.

However, in this experiment it is not possible to separate the Reynolds analogy factor from the form factor. We could in fact regard intermediate enthalpy as being in fair agreement with a Reynolds analogy factor of 1.22 for a form factor of 1.05 instead of 1.18, that is for a value intermediate between that suggested by Van Driest²⁰ or Young¹⁹ and that claimed by Buglia²¹ for blunt cones.

6. Heat Transfer to Hemispheres.

6.1. Local-flow Conditions.

Local flow conditions for the hemispheres were derived on the assumptions of normal-shock total-pressure loss at the nose, isentropic flow from the stagnation point over the surface just outside the boundary layer, and the Newtonian static pressure distribution

$$p_1 = p_s \cos^2\theta + p_\infty \sin^2\theta$$

where θ corresponds to the geodetic latitude with respect to the stagnation point as pole; and p is the static pressure.

Suffixes ∞ , s , 1 refer to free stream, stagnation point, and local conditions just outside the boundary layer respectively.

6.2. Theoretical Predictions.

The measured heat-transfer data were compared with those predicted by the methods of Stine and Wanlass² for laminar flow, and by Peattie and Wild³ and Van Driest⁴ for turbulent flow with the modifications indicated below.

Laminar flow. A recovery factor of 0.88 was assumed as for turbulent flow instead of a more plausible lower value¹. However this was of little significance since for the most part, M_1 was small at the relevant stations (see equation (5)). The significant parameter used by Stine and Wanlass is the Nusselt number divided by the root of the Reynolds number evaluated at conditions just outside the boundary layer.

The Nusselt number,

$$Nu = qx / (T_{wo} - T_w)k.$$

Turbulent flow. The basis of estimation for turbulent flow was similar to that described in Section 5 for the conical case taking a Reynolds analogy factor of 1.22. Air viscosity and density were relevant to intermediate enthalpy. The form factor, f , however was modified to take account of the variable velocity gradient on the hemisphere.

In one estimate it was assumed to conform to the relation proposed by Peattie and Wild³, i.e. it is independent of Mach number and varies with angle from 1.20 at the stagnation point to 0.98 at $\theta = 90^\circ$.

In the other we assumed the form factor was a more definite function of the actual velocity distribution in a way similar to that preferred by Van Driest⁴. However, instead of taking f as varying linearly with

u_1/x , we felt that it was preferable to assume linearity with du_1/dx . The constants of linearity were so defined, that at the shoulder ($\theta = 90^\circ$) the flat plate value of 1 obtained, and that close to stagnation the value was 1.42 (as demonstrated by Van Driest for a turbulent velocity profile).

6.3. Experimental Results.

Experimental heat-transfer data were obtainable from four out of the five hemispherical heads namely, heads 5, 6, 8 and 9. Details of the trajectory data are given in Figs. 18 a to d, temperature histories in Figs. 19a to d and heat-transfer rate histories in Figs. 20b to e respectively. Estimated local Reynolds number histories for head 5 are shown in Fig. 21.

Temperature histories at the three stations in the insulating air gap of head 9 are given in Fig. 22a. Estimates based on these suggest that the maximum heat loss to the interior may have been as high as 2 C.H.U./ft² sec. Comparable temperature histories for the internal air at axial stations for the uninsulated head 8 are given in Fig. 22b.

The temperature data for the various thermocouple stations of the head walls have been reduced to local Stanton number, k_H , or local N_u/\sqrt{R} , except in the case of head 9 where up to the present only N_u/\sqrt{R} for the stagnation point has been evaluated.

Stagnation point. Figs. 26a and 26b show the variation of N_u/\sqrt{R} at the stagnation points for the 10 inch and 4 inch hemispheres respectively. The theoretical value* of 0.67 given by Stine and Wanlass² for this ratio is indicated and in Fig. 26b the approximate limits of the 99% uncertainty range relevant to the random errors of the basic data for head 9 is also shown. The plots suggest fair agreement with the theoretical value—better for the 10 inch than for the 4 inch hemisphere data.

Transition and laminar flow. From a comparison of the experimental data with the theoretical predictions of Refs. 2, 3 and 4, it was possible at most of the stations to identify the local flow regime as either laminar or turbulent. The local regimes so deduced are tabulated in Table 3 and shown diagrammatically in Fig. 27. The values of N_u/\sqrt{R} identified with laminar flow ranged on the average from about the values* predicted by Ref. 2 to about 1.5 times these values. The approximate values of this ratio are indicated in Fig. 27 for the five relevant stations. They do not seem to be correlated with angle.

On the smooth 10 inch hemisphere (head 5) the flow over meridian 0° remained laminar at latitude 30° until 2.75 sec; $R = 3 \times 10^6$, $h_w/h_1 = 0.445$, $M_1 = 0.63$ (Fig. 28a). On the 180° meridian the flow was apparently turbulent at latitude 45° until 2.63 sec; $R = 5.3 \times 10^6$, $h_w/h_1 = 0.497$, $M_1 = 0.98$, when the heat-transfer coefficient, N_u/\sqrt{R} , indicated transition to laminar flow (Fig. 28b), the flow remaining laminar for the rest of the record (i.e. up to 4.2 sec). The apparent evidence of turbulent flow at station (45°, 180°) may however be only a manifestation of the transient accuracy of the measurement at that time. Elsewhere no changes in the heat-transfer rates of magnitudes compatible with transition was detected.

The asymmetric location of transition relative to the stagnation point was noted on both 10 inch hemispheres (heads 5 and 6). On occasions the latitude of transition on the 0° meridian was less than 30° while at the same instant it was at least 45° on the 180° meridian (Fig. 27).

Turbulent flow. Experimental values of Stanton number, k_H , are presented in a two-way tabulation against Mach number and angle in Tables 4a to 4c for heads 5, 6 and 8 respectively together with the predictions based on Van Driest⁴ and Peattie and Wild³ for turbulent flow. It can be seen that on the whole, the predictions based on Peattie and Wild are closer to the experimental values than those based on Van Driest. The data for each hemisphere seem to be well correlated by a plot against angle of the ratio of experimental Stanton numbers, k_H , to those predicted by Peattie and Wild³ measured over

*The theoretical values quoted are actually relevant to $M_\infty = 1.97$. They should not change appreciably at higher Mach numbers until dissociation is encountered.

the Mach number range (Fig. 29a). For the smooth 10 inch hemisphere, this ratio at most of the stations is about 0.8—the values at $(45^\circ, 0^\circ)$ and $(90^\circ, 0^\circ)$ are markedly different. On the other hand, there is a marked variation with angle for the rough 10 inch hemisphere from about 1.25 at 30° to about 1 at 90° and for the 4 inch hemisphere from about 0.5 at 45° to about 0.8 at 90° . It is interesting to note that the laminar flow values for the ratio tend to collapse onto a common curve and that (with some irregularities) the turbulent flow values for the 4 inch hemisphere tend to flow back into this curve without discontinuity. There is a suggestion too that the values for the smooth 10 inch hemisphere have a similar trend. It is also interesting to note that the value at the anomalous point at $(45^\circ, 0^\circ)$ on the rough 10 inch hemisphere is compatible with the trend for the 4 inch hemisphere.

In Fig. 29b, the means of the ratio for turbulent flow with respect to angle have been plotted against Mach number. We find in the case of the 10 inch hemispheres there is little variation with Mach number whereas for the 4 inch hemisphere, for which the Mach number stretch is wider, there is a marked difference between the levels at the higher and lower Mach numbers. The level at Mach numbers up to 3 is about 0.6 times the level at the higher Mach numbers, this latter level being compatible with that for the smooth 10 inch hemisphere.

The ratio of mean values for the rough and smooth 10 inch hemispheres is about 1.3; which is of the order of the factor given by Royal Aeronautical Data Sheets²⁷ for the increase of skin friction at subsonic speeds corresponding to the roughness of the surface finish.

7. Conclusions.

7.1. Cone.

Theory¹ based on intermediate enthalpy, a Reynolds analogy factor of 1.22 and a form factor of 1.18 overestimated the heating rates by about 12% on the average. This trend is in conformity with American experience. The possibility that heat loss to the interior may account for the discrepancy cannot be excluded.

7.2. Hemispheres.

The data relative to hemispherical heads indicate the following results:

(i) Fair agreement is obtained with the theory of Stine and Wanlass² at the stagnation point and some agreement at those stations identified with laminar flow.

(ii) On the whole, predictions for turbulent heat-transfer on the basis of Peattie and Wild³ are closer than those on the basis of Van Driest⁴ but neither give a satisfactory correlation of all the data.

(iii) The roughness of the surface finish can give rise to an appreciable increase in turbulent heat-transfer rate. A 10 inch diameter hemisphere with a C.L.A. finish of 200 microinches was found to have turbulent heat-transfer rates about 30% greater on the average than those of a similar smooth one.

(iv) The distance of the boundary between laminar and turbulent flow from the nose was not the same along different streamlines radiating from the stagnation point.

LIST OF SYMBOLS

Air Properties

T	Temperature
h	Enthalpy
μ	Viscosity
ρ	Density
p	Pressure
u	Velocity
q	Local rate of heat transfer per unit area from the boundary layer to the head
k	Thermal conductivity

Head

σ	Wall specific heat
τ	Wall thickness
τ_0	Wall thickness at 15°C
δ	Wall density
G	Heat capacity of wall per unit area
x	Wetted distance from stagnation point on hemisphere or apex on cone (<i>see</i> Fig. 16)
D	Diameter of hemisphere
θ	Angular co-ordinate of point on the surface of a hemisphere relative to the stagnation point (<i>Fig. 16</i>)
ϕ	Angular co-ordinate of point on the surface of a hemisphere relative to some reference meridian through the stagnation point, and also on cone with respect to reference plane containing axis (<i>see</i> Fig. 16)

} θ and ϕ correspond to the latitude and longitude of geodesy with respect to the stagnation point as pole

Dimensionless values

M	Mach number
R^*	Local Reynolds number $\left(= \frac{\rho^* u_1 x}{\mu^*} \right)$ relative to some boundary layer reference enthalpy

LIST OF SYMBOLS—*continued*

R	Local Reynolds number $\left(= \frac{\rho_1 u_1 x}{\mu_1} \right)$ relative to conditions just outside boundary layer
C_f	Local skin-friction coefficient
N_u	Local Nusselt number $= \frac{q x}{(T_{wo} - T_w) k}$
k_H	Local Stanton number $\left(= \frac{q}{\rho_1 u_1 (h_{wo} - h_w)} \right)$ relative to density evaluated just outside boundary layer
k_H^*	Local Stanton number $\left(= \frac{q}{\rho^* u_1 (h_{wo} - h_w)} \right)$ relative to density evaluated at some boundary layer reference enthalpy
r	Recovery factor $= \frac{2}{(\gamma - 1) M_1^2} \left(\frac{h_{wo}}{h_1} - 1 \right)$
s	Reynolds analogy factor $= \frac{k_H}{\frac{1}{2} C_f}$
f	Form factor
<i>Superscript</i>	
*	Reference enthalpy, or evaluated at reference enthalpy
<i>Suffices</i>	
∞	Undisturbed flow ahead of shock wave or body
1	Local conditions in the stream outside the boundary layer
w	At surface temperature conditions
wo	At surface temperature for zero heat transfer
s	Stagnation conditions

REFERENCES

- | <i>No.</i> | <i>Author(s)</i> | <i>Title, etc.</i> |
|------------|---|--|
| 1 | R. J. Monaghan | Formulae and approximations for aerodynamic heating rates in high speed flight.
A.R.C. C.P.360. October, 1955. |
| 2 | H. A. Stine and
K. Wanlass | Theoretical and experimental investigation of aerodynamic heating and isothermal heat-transfer parameters on a hemispherical nose with laminar boundary layer at supersonic Mach numbers.
N.A.C.A. Tech. Note 3344. December, 1954. |
| 3 | I. W. Peattie and N. E. Wild | Unpublished M.O.A. Report. |
| 4 | E. R. Van Driest | The problem of aerodynamic heating.
<i>Aeronautical Engineering Review</i> . October, 1956. |
| 5 | H. G. R. Robinson
and G. S. Barford | The C.T.V.5 series 2 kinetic heating test vehicle.
R.A.E. Tech. Note G.W.456. June, 1957. |
| 6 | J. H. T. Wade | An experimental investigation of the effect of surface roughness on the drag of a cone-cylinder model at a Mach number of 2.48.
<i>Canadian Aeronautical Journal</i> , Vol. 2, No. 8, p. 291. October, 1956. |
| 7 | V. M. Hickson | The welding of thermocouple junctions.
<i>Journal of Scientific Instruments</i> , Vol. 17, pp. 182 to 186. July, 1940. |
| 8 | M. Cooper and E. E. Mayo | Normal conduction effects on heat-transfer data during transient heating of thin skin models.
<i>Journal of Aeronautical Sciences</i> , Vol. 24, No. 6, p. 461. June, 1957. |
| 9 | R. N. C. Strain and
J. H. Sewell | The use of Sirasil cement for high temperature resistance strain gauges.
R.A.E. Tech. Memo. Chem. 130. |
| 10 | W. Walters and D. Walker | Further experiments in temperature measuring technique involving mixture of low level signal with variable inductance transducer output.
Unpublished M.O.A. Report. |
| 11 | E. R. G. Eckert | Survey on heat-transfer at high speeds.
Transactions of the <i>American Society of Mechanical Engineers</i> , Vol. 78, pp. 1273 to 1284. August, 1956. |
| 12 | R. L. Dommett, D. I. Dawton
and R. A. Harrison | C.T.V.5 Series 2 analysis of heating data for seven firings.
R.A.E. Tech. Note G.W.515. May, 1959. |
| 13 | — | <i>Physical constants of some commercial steels at elevated temperatures.</i>
Edited by B.I.S.R.A. Butterworth Scientific Publications. 1953. |
| 14 | E. Whittaker and
G. Robinson | <i>The calculus of observation.</i>
Blackie & Son, 4th edition. 1954. |

REFERENCES—*continued*

- | <i>No.</i> | <i>Author(s)</i> | <i>Title, etc.</i> |
|------------|--|---|
| 15 | J. K. Sterret | Manual for moving polynomial arc smoothing.
U.S.A. Ballistic Research Lab. Report 840. November, 1952. |
| 16 | J. Picken | Notes on a reduction procedure for temperature data from free flight telemetry.
Unpublished M.O.A. Report. |
| 17 | R. J. Monaghan,
J. F. W. Crane and
J. Picken | Research in Aerodynamics Department, R.A.E. on the problems of aerodynamic heating.
Unpublished M.O.A. Report. |
| 18 | R. J. Monaghan | A review and assessment of various formulae for turbulent skin friction in compressible flow.
A.R.C. C.P.142. August, 1952. |
| 19 | A. D. Young | The calculation of the profile drag of aerofoils and bodies of revolution at supersonic speeds.
College of Aeronautics, Cranfield, Report 73. April, 1953. |
| 20 | E. R. Van Driest | Turbulent boundary layer on a cone in supersonic flow at zero angle of attack.
<i>Journal of the Aeronautical Sciences</i> , Vol. 19, No. 1, p. 55. January, 1952. |
| 21 | J. J. Buglia | Heat transfer and boundary-layer transition on a highly polished hemisphere-cone in free flight at Mach numbers up to 3.14 and Reynolds numbers up to 24×10^6 .
N.A.S.A. Tech. Note D-955. September, 1961. |
| 22 | — | Tables of supersonic flow about cones.
M.I.T. Tech. Report 1, Cambridge, Massachusetts. 1947. |
| 23 | C. B. Rumsay, R. O. Piland
and R. N. Hopko | Aerodynamic-heating data obtained from free-flight tests between Mach numbers of 1 and 5.
N.A.C.A. Research Memo. L55A14a. TIB 4615. March, 1955. |
| 24 | L. Rabb and
S. H. Simpkinson | Free-flight heat-transfer measurements on two 20°-cone-cylinders at Mach numbers from 1.3 to 4.9.
N.A.C.A. Research Memo E55F27. TIB 4746. July, 1955. |
| 25 | C. B. Rumsay and D. B. Lee | Measurements of aerodynamic heat transfer and boundary-layer transition on a 10° cone in free flight at supersonic Mach numbers up to 5.9.
N.A.S.A. Tech. Note D-745. May, 1961. |
| 26 | A. Seiff | Examination of the existing data on the heat transfer of turbulent boundary layers at supersonic speeds from the point of view of Reynolds analogy.
N.A.C.A. Tech. Note 3284. August, 1954. |
| 27 | — | Data sheets Section: Wings 02.04.08.
Issued by the Royal Aeronautical Society. August, 1956. |

TABLE 1

Physical data for typical vehicle

(conical head 10)

Gross weight at launching		704 lb
Gross weight of rocket motor with fuel		523 lb
Weight of fin and flare assembly		53 lb
Weight of components forward of rocket motor		128 lb
Breakdown of weights of components forward of rocket motor	{ Measuring head Telemetry components Outer case Bulkheads and internal structure Ballast	3 lb
		18 lb
		36 lb
		44 lb
		27 lb
Overall length of vehicle		177.4 inches
Centre of gravity	at launching	97.9 inches
aft of vertex of cone	during coasting	87.4 inches
Nett fin area (two fins)		331.0 sq. in.

TABLE 2

Summary of Flights Made between 9.2.56 and 9.7.57

Serial No.	1	2	3	4	5	6	7	8	9	10
Date	9.2.56	12.4.56	9.6.56	21.8.56	22.8.56		10.12.56	11.12.56	11.3.57	9.7.57
All up weight before firing (lb)	702	680	682	692	660	695	712	711	712	704
Purpose	Proving vehicle design	Proving temperature instrumentation	Investigating reference enthalpy	Investigating boost and telemetry failures	Kinetic heating and transition on hemispheres					Repeat of vehicle 3
Main measurements	Longitudinal and lateral acceleration	Temperature at 6 stations on head		Temperature at 2 stations on head and 4 stations inside head	Temperature at 11 stations on head	Temperature at 9 stations on head	Temperature at 9 stations on head and 3 of insulation air gap	Temperature at 9 stations on head and 3 of air inside head	As for head 7	Temperature at 10 stations on head and 2 of air inside head
Head shape	Slim cone				10 inch diameter hemisphere cylinder		4 inch diameter hemisphere cylinder			Slim cone
Mean wall thickness (inches)	0.125	0.024			0.047		0.062	0.060	0.066	0.034
Insulation	None	Glass wool	Durestos discs		Durestos channel		Durestos inner wall with air gap of 0.1 in.	None	As for vehicle 7	
Method of manufacture	Fabricated from mild steel sheet									Machined from solid
Roughness C.L.A. (microinches)	Not measured		17 to 31		3.5	200	4.0			
Maximum velocity (f/s)	5350	5434	5420	5210	4830	4520	—	> 5000	5100	5150
Maximum Mach number	4.96	4.95	4.90	4.72	4.37	4.09	—	> 4.53	4.52	4.66
Time to maximum velocity (sec)	3.23	3.54	3.70	3.80	3.45	3.58	—	> 3.5	3.24	3.52
Duration of useful record (sec)	0 to 4.1	0	0 to 3.1	0	0 to 4.3	0 to 4.6	0	0 to 3.5	0 to 10.7	3.0 to 10.0
Primary limiting factor	Explosion in rocket motor	Telemetry failure			Kiné-theodolite failed to follow		Ground instrumentation failure	Kiné-theodolite failed to follow	—	Telemetry failure for first 3 sec of flight

TABLE 3

Location of Stations, Local Wall Thickness and Flow Regimes for Walls of Heads 3, 5, 6 and 8

Conical head 3

Station Ref. No.	Location of station*		Local wall thickness inches	Flow Degime
	x inches	ϕ degrees		
1	3.7	0	0.0232	Turbulent
2	7.0	0	0.0221	"
3	12.0	0	0.0237	"
4a	16.0	0	0.0241	"
4b	16.0	0	0.0241	"
5	16.0	120	0.0240	"
6	16.0	240	0.0240	"

TABLE 3—continued

Hemisphere cylinders (heads 5, 6 and 8)

Head Ref. No.	Diameter inches	Station Ref. No.	Location of station*			Local wall thickness inches	Flow Regime
			x	θ degrees	ϕ degrees		
5	10	1	1.45 D	0	0	0.0513	—
		2		30	0	0.0469	Laminar till $t = 2.7$ sec then turbulent
		3		40	0	0.0471	Turbulent
		4		45	0	0.0471	"
		5		45	180	0.0487	Laminar from $t = 2.5$, perhaps turbulent till $t = 2.4$
		6		50	0	0.0471	Turbulent
		10		55	0	0.0470	"
		7		60	0	0.0469	"
		11		70	0	0.0472	"
	8	90	0	0.0469	"		
	9	—	0	0.0532	"		
6	10	1	1.45 D	0	0	0.0573	—
		2		30	0	0.0488	Turbulent
		3		40	0	0.0468	"
		4		45	0	0.0458	"
		5		45	180	0.0490	Laminar
		6		50	0	0.0455	Turbulent
		7		60	0	0.0453	"
		8		90	0	0.0523	"
		9		—	0	0.0527	"
8	4	1	1.45 D	0	0	0.0577	—
		2		15	0	0.0582	Laminar
		3		30	0	0.0596	"
		4		45	0	0.0592	Turbulent perhaps laminar from $t = 2.16$ to 2.30
		5		50	0	0.0593	Turbulent
		6		60	0	0.0584	"
		7		75	0	0.0578	"
		8		90	0	0.0598	"
		9		—	0	0.0657	"

*The co-ordinate system is defined in Fig. 16.

TABLE 4a

Predicted and Experimental Values of Stanton Number, k_H , vs. Location of Station and Free-Stream Mach Number

Smooth 10 inch hemisphere (head 5) k_H in units of 10^{-3}

Free-stream Mach number				2.75	3.0	3.25	3.50	3.75	4.0	4.25	4.25	4.0	3.75	3.6
Location of station*														
x	θ	ϕ	Source of value [†]	← Acceleration →						← Deceleration →				
	30°	0°	VD	3.26	3.26	3.24	3.22	3.16	3.09	3.03	2.92	2.86	2.80	2.78
			P & W	2.64	2.66	2.66	2.64	2.59	2.55	2.50	2.42	2.36	2.31	2.28
			Exp {	0.84	0.73	0.77	1.93	1.88	1.85	1.73	0.86	-0.20	-0.27	-0.50
				0.81	0.72	0.94	1.93	1.81	1.87	1.79	0.74	-0.12	-0.29	-0.29
	40°	0°	VD	2.87	2.85	2.82	2.80	2.77	2.75	2.72	2.60	2.50	2.42	2.38
			P & W	2.30	2.28	2.26	2.25	2.24	2.23	2.21	2.11	2.03	1.96	1.92
			Exp {	1.71	1.88	1.74	1.44	1.50	1.54	1.47	1.80	1.65	0.29	
				1.66	1.70	1.65	1.55	1.54	1.49	1.51	1.85	1.55	0.62	
	45°	0°	VD	2.74	2.72	2.70	2.68	2.65	2.63	2.60				
			P & W	2.18	2.16	2.15	2.14	2.12	2.11	2.10				
			Exp {	1.82	1.71	1.72	1.52	1.46	1.64	1.64				
				1.88	1.79	1.56	1.50	1.61	1.61	1.62				
	45°	180°	VD	2.83	2.81	2.85	2.86	2.86	2.84	2.87	2.82	2.76	2.68	2.66
			P & W	2.24	2.24	2.27	2.29	2.29	2.28	2.31	2.26	2.22	2.16	2.12
			Exp {	0.97	0.41	0.34	0.35	0.33	0.33	0.35	0.38	0.41	0.45	0.47
				0.99	0.47	0.29	0.32	0.37	0.35	0.32	0.42	0.38	0.37	

TABLE 4a—continued

Predicted and Experimental Values of Stanton Number, k_H , vs. Location of Station and Free-Stream Mach Number

Smooth 10 inch hemisphere (head 5) k_H in units of 10^{-3}

Free-stream Mach number				2.75	3.0	3.50	3.50	3.75	4.0	4.25	4.25	4.0	3.75	3.6
Location of station*														
x	θ	ϕ	Source of value [†]	← Acceleration →						← Deceleration →				
	50°	0°	VD	2.64	2.62	2.60	2.58	2.57	2.56	2.54				
			P & W	2.07	2.06	2.05	2.04	2.04	2.04	2.03				
			Exp {	1.70	1.68	1.58	1.42	1.42	1.50	1.51				
				1.79	1.62	1.54	1.44	1.44	1.50	1.51				
	55°	0°	VD	2.54	2.52	2.51	2.50	2.50	2.49	2.47				
			P & W	1.98	1.97	1.97	1.96	1.95	1.95	1.94				
			Exp {	1.86	1.63	1.42	1.33	1.37	1.48	1.44				
				1.69	1.59	1.54	1.39	1.37	1.45	1.40				
	60°	0°	VD	2.43	2.43	2.44	2.42	2.43	2.42	2.41	2.32	2.20	2.12	2.04
			P & W	1.88	1.88	1.88	1.88	1.88	1.88	1.87	1.78	1.70	1.64	1.58
			Exp {	1.38	1.52	1.47	1.39	1.39	1.44	1.40	1.47	1.48	1.61	1.60
				1.47	1.52	1.49	1.45	1.45	1.51	1.41	1.59	1.79	1.09	
	70°	0°	VD	2.15	2.19	2.22	2.25	2.27	2.29	2.30	2.20	2.09	2.00	1.95
			P & W	1.71	1.72	1.74	1.74	1.75	1.76	1.76	1.68	1.60	1.54	1.51
			Exp {	1.21	1.35	1.40	1.23	1.26	1.39	1.36	1.57	1.51	0.72	0.64
				1.39	1.24	1.33	1.27	1.34	1.44	1.38	1.56	1.57	0.87	0.63

TABLE 4a—continued

Predicted and Experimental Values of Stanton Number, k_H , vs. Location of Station and Free-Stream Mach Number

Smooth 10 inch hemisphere (head 5) k_H in units of 10^{-3}

Free-stream Mach number				2.75	3.0	3.50	3.50	3.75	4.0	4.25	4.25	4.0	3.75	3.6
Location of station*				← Acceleration →						← Deceleration →				
x	θ	ϕ	Source of value [†]											
0.785 D	90°	0°	VD	1.45	1.46	1.46	1.48	1.50	1.52	1.52	1.49	1.42	1.36	1.34
			P & W	1.42	1.43	1.43	1.45	1.47	1.48	1.50	1.46	1.38	1.34	1.32
			Exp {	1.59	1.34	1.13	1.30	1.38	1.43	1.56	1.84	1.80	0.41	0.02
				1.41	1.28	1.12	1.20	1.38	1.48	1.59	1.98	1.55	0.58	
1.45 D	—	0°	Flat Plate	1.32	1.33	1.35	1.36	1.38	1.40	1.41	1.38	1.32	1.28	1.26
			Exp {	0.92	0.86	0.92	1.00	1.12	1.18	1.21	1.25	1.11	1.12	0.63
				0.83	0.83	0.77	0.99	1.16	1.15	1.16	1.37	1.28	0.91	

* The co-ordinate system is defined in Fig. 16. † VD designates Van Driest (Ref. 4). P & W designate Peattie and Wild (Ref. 3).

Exp designates experimental value. The relevant temperature data were split into two interlacing sets which were separately processed and used in the subsequent analysis. Both sets of results are included in the table for the experimental data. The differences between them give a measure of the inaccuracy arising from reading the records.

TABLE 4b

Predicted and Experimental Values of Stanton Number, k_H , vs. Location of Station and Free-Stream Mach Number

Rough 10 inch hemisphere (head 6) k_H in units of 10^{-3}

Free stream Mach No.				3.0	3.25	3.5	3.75	4.0	4.0	3.75	3.5
Location of station*											
x	θ	ϕ	Source of value [†]	← Acceleration →				← Deceleration →			
	30°	0°	VD P & W Exp {	3.01 2.45 3.05 3.05	2.96 2.43 2.91 2.82						
	40°	0°	VD P & W Exp {	2.71 2.18 2.03 2.42	2.69 2.16 2.23 2.25	2.68 2.16 2.25 2.16	2.65 2.14 2.00 2.09	2.61 2.12 2.89 2.94			
	45°	0°	VD P & W Exp {	2.73 2.17 1.40 1.26	2.70 2.16 1.35 1.38	2.68 2.14 1.24 1.46	2.66 2.13 1.10 1.10	2.66 2.10 0.93 0.92	2.62 2.02 0.78 0.94	2.52 2.02 0.64 0.62	2.48 1.94 0.13
	45°	180°	VD P & W Exp {	2.84 2.25 0.45 0.47	2.83 2.26 0.47 0.53	2.83 2.26 0.52 0.48	2.85 2.28 0.41 0.45	2.87 2.30 0.43 0.43	2.84 2.28 0.34 0.37	2.76 2.22 0.27 0.30	2.70 2.16 0.10 0.14
	50°	0°	VD P & W Exp {	2.44 1.98 2.27 2.38	2.38 1.96 2.24 2.29						
	60°	0°	VD P & W Exp {	2.37 1.84 2.02 1.92	2.37 1.84 1.95 1.78	2.35 1.82 1.85 1.92	2.32 1.80 1.69 1.80	2.33 1.81 1.65 1.65			
0.785 D	90°	0°	VD P & W Exp {	1.47 1.44 1.14 1.23	1.48 1.45 1.41 1.54	1.49 1.46 1.43 1.50	1.50 1.47 1.44 1.53	1.51 1.48 1.58 1.63	1.48 1.46 1.80 1.87	1.42 1.38 1.97 1.72	1.36 1.32 1.76 1.66

TABLE 4b

Predicted and Experimental Values of Stanton Number, k_H , vs. Location of Station and Free-Stream Mach Number

Rough 10 inch hemisphere (head 6) k_H in units of 10^{-3}

Free stream Mach No.				3.0	3.25	3.5	3.75	4.0	4.0	3.75	3.5
Location of station*				← Acceleration →					← Deceleration →		
x	θ	ϕ	Source of value †								
1.45 D	—	0°	Flat Plate	1.33	1.34	1.35	1.36	1.38	1.35	1.30	1.26
			Exp {	1.34	1.26	1.32	1.50	1.40	1.68	1.64	1.26
				1.26	1.03	1.15	1.37	1.52	1.59	1.52	1.44

*The co-ordinate system is defined in Fig. 16. †VD designates Van Driest (Ref. 4).
P & W designates Peattie and Wild (Ref. 3). Exp designates experimental value.

The relevant temperature data were split into two interlacing sets which were separately processed and used in the subsequent analysis. Both sets of results are included in the table for the experimental data. The differences between them give a measure of the inaccuracy arising from reading the records.

TABLE 4c

Predicted and Experimental Values of Stanton Number, k_H , vs. Location of Station and Free-Stream Mach Number

4 inch hemisphere (head 8) k_H in units of 10^{-3}

Free stream Mach No.				2.0	2.25	2.5	2.75	3.0	3.25	3.5	3.75	4.0	4.25	4.5
Location of station*				← Acceleration →							← Deceleration →			
x	θ	ϕ	Source of value [†]											
	15°	0°	VD	5.02	4.94	4.87	4.84	4.81	4.79	4.76	4.72	4.69	4.64	4.57
			P & W	3.98	3.97	3.96	3.96	3.96	3.96	3.95	3.94	3.92	3.89	3.84
			Exp {	2.45	1.69	1.55	1.31	1.43	1.68	1.67	1.67	1.54	1.60	1.74
				1.91	1.60	1.60	1.63	1.61	1.53	1.58	1.58	1.54	1.70	1.72
	30°	0°	VD	3.88	3.84	3.79	3.77	3.76	3.75	3.74	3.72	3.70	3.67	3.61
			P & W	3.03	3.04	3.05	3.05	3.06	3.06	3.07	3.07	3.05	3.04	3.00
			Exp {	0.92	1.14	1.24	1.13	0.92	0.92	0.87	0.98	0.90	0.92	0.79
				0.85	1.33	1.07	0.95	0.90	0.92	0.93	1.01	0.93	0.90	0.80
	45°	0°	VD	3.27	3.24	3.23	3.24	3.24	3.24	3.22	3.19	3.15	3.11	3.05
			P & W	2.54	2.54	2.56	2.57	2.58	2.58	2.57	2.55	2.53	2.57	2.47
			Exp {	1.34	1.22	0.84	0.52	0.90	1.22	1.44	1.55	1.53	1.45	1.25
				1.45	1.32	0.89	0.57	0.85	1.12	1.43	1.51	1.59	1.43	1.21
	50°	0°	VD	3.13	3.10	3.10	3.11	3.12	3.11	3.10	3.08	3.05	2.99	2.94
			P & W	2.42	2.42	2.43	2.44	2.46	2.46	2.46	2.44	2.41	2.38	2.34
			Exp {	1.07	1.21	1.03	0.85	1.00	1.32	1.48	1.60	1.51	1.37	1.16
				1.01	1.20	1.07	0.83	0.98	1.22	1.49	1.67	1.51	1.41	1.18
	60°	0°	VD	2.84	2.83	2.84	2.86	2.88	2.88	2.88	2.88	2.87	2.85	2.79
			P & W	2.20	2.20	2.20	2.22	2.23	2.23	2.23	2.23	2.22	2.20	2.16
			Exp {	1.54	1.22	0.98	0.73	0.84	1.24	1.48	1.57	1.56	1.72	1.55
				1.62	1.40	0.97	0.74	0.93	1.07	1.49	1.57	1.54	1.68	1.53

TABLE 4c—continued

Predicted and Experimental Values of Stanton Number, k_H , vs. Location of Station and Free-Stream Mach Number4 inch hemisphere (head 8) k_H in units of 10^{-3}

Free stream Mach No.				2.0	2.25	2.5	2.75	3.0	3.25	3.5	3.75	4.0	4.25	4.5
Location of station*				← Acceleration →							← Deceleration →			
x	θ	ϕ	Source of value [†]											
	75°	0°	VD	2.37	2.39	2.43	2.47	2.52	2.56	2.59	2.61	2.63	2.65	2.63
			P & W	1.92	1.92	1.92	1.94	1.97	1.98	1.99	1.99	1.99	1.99	1.97
			Exp {	0.76	0.83	0.84	0.87	1.11	1.31	1.65	1.71	1.65	1.71	1.53
				0.87	0.93	0.79	0.87	0.99	1.31	1.62	1.80	1.69	1.72	1.55
0.785 D	90°	0°	VD	1.72	1.71	1.71	1.72	1.74	1.76	1.77	1.79	1.81	1.82	1.81
			P & W	1.68	1.67	1.68	1.69	1.70	1.72	1.74	1.75	1.77	1.78	1.77
			Exp {	0.95	1.12	0.79	0.94	0.73	1.21	1.46	1.79	1.98	2.28	2.26
				1.18	0.95	0.89	0.84	0.94	1.01	1.51	1.64	1.90	2.41	2.37
1.45 D	—	0°	Flat plate	1.56	1.55	1.55	1.57	1.58	1.60	1.61	1.63	1.65	1.66	1.66
			Exp {	0.98	1.05	0.56	0.73	0.83	1.24	1.49	1.62	1.52	1.57	1.48
				0.63	0.78	0.57	0.33	0.66	1.24	1.49	1.80	1.67	1.51	1.50

*The co-ordinate system is defined in Fig. 16. [†]VD designates Van Driest (Ref. 4). P & W designates Peattie and Wild (Ref. 3).

Exp designates experimental value. The relevant temperature data were split into two interlacing sets which were separately processed and used in the subsequent analysis. Both sets of results are included in the table for the experimental data. The difference between them give a measure of the inaccuracy arising from reading the records.

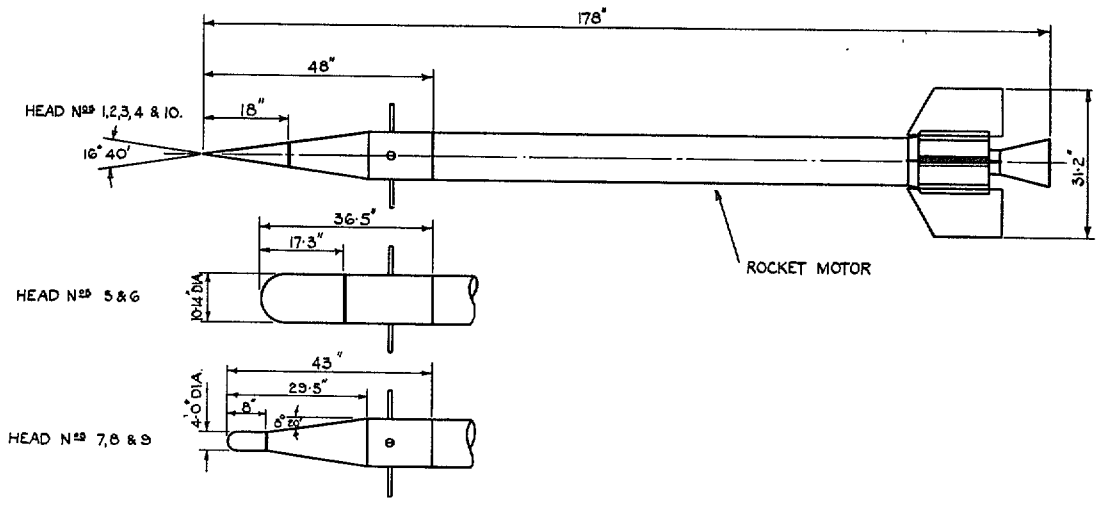


FIG. 1. Sketch of test vehicles.

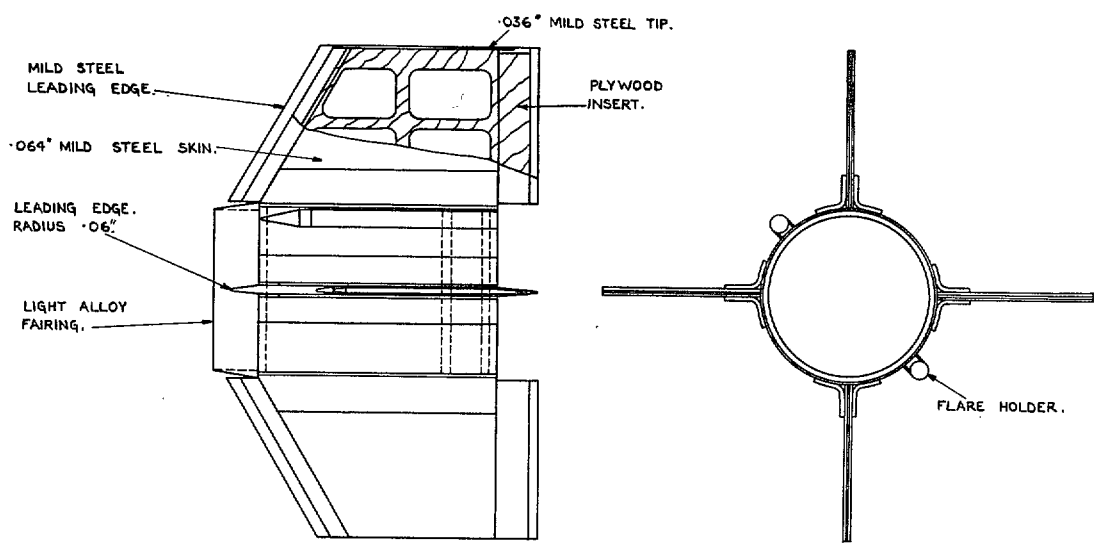


FIG. 2. Fin assembly.

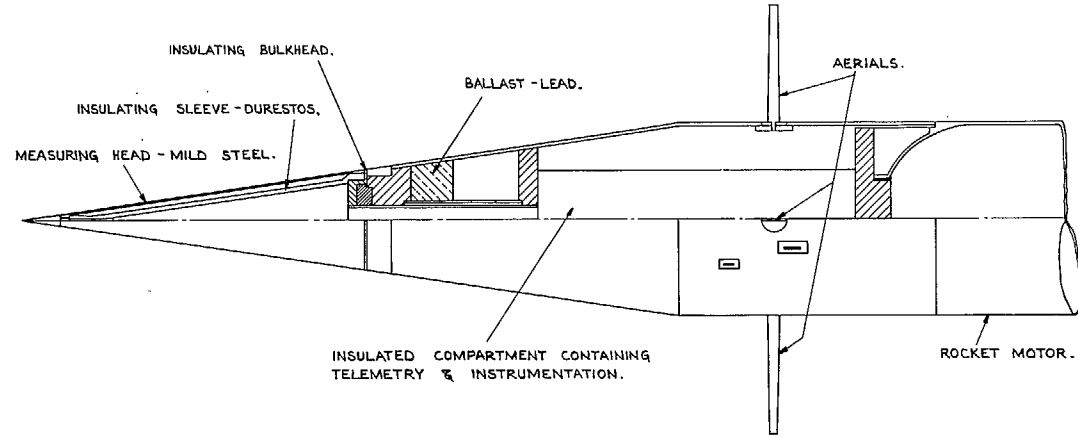


FIG. 3. Head and instrumentation assembly.

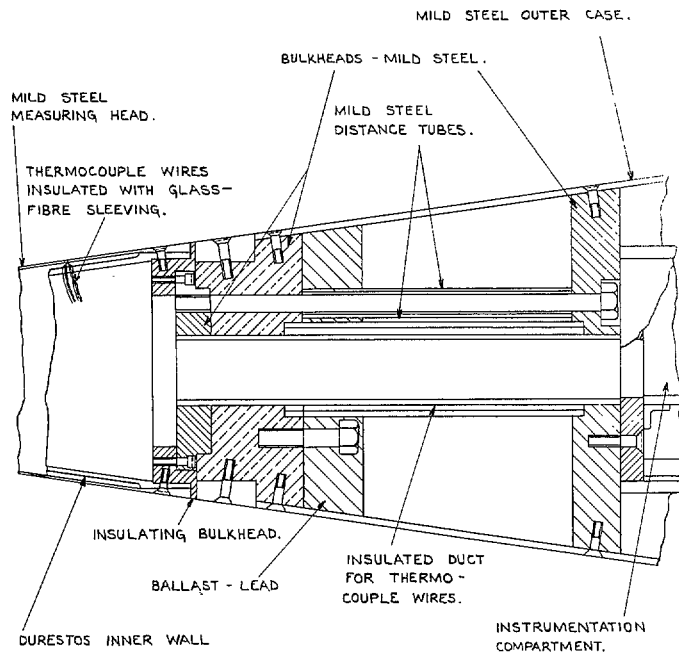


FIG. 4a. Details of junction of measuring head with instrumentation compartment.

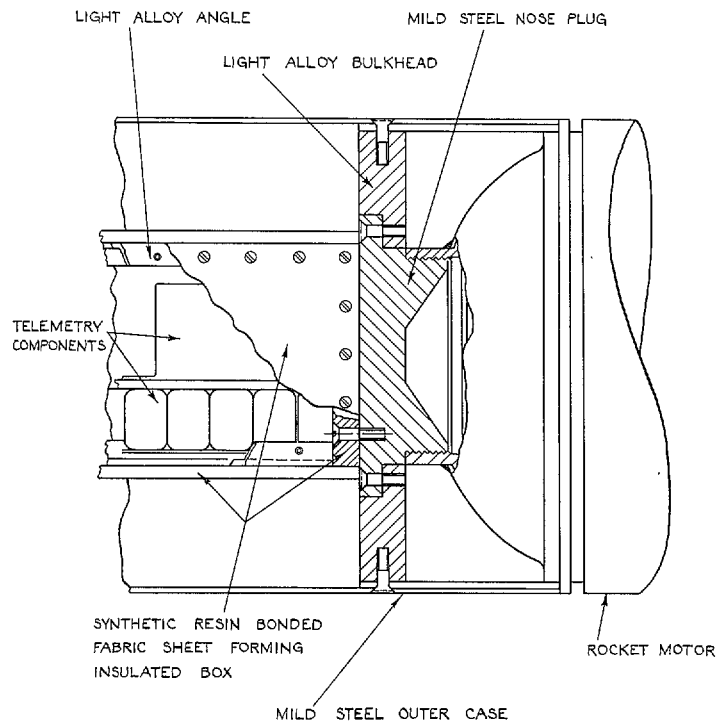


FIG. 4b. Details of junction of instrumentation compartment with rocket motor.

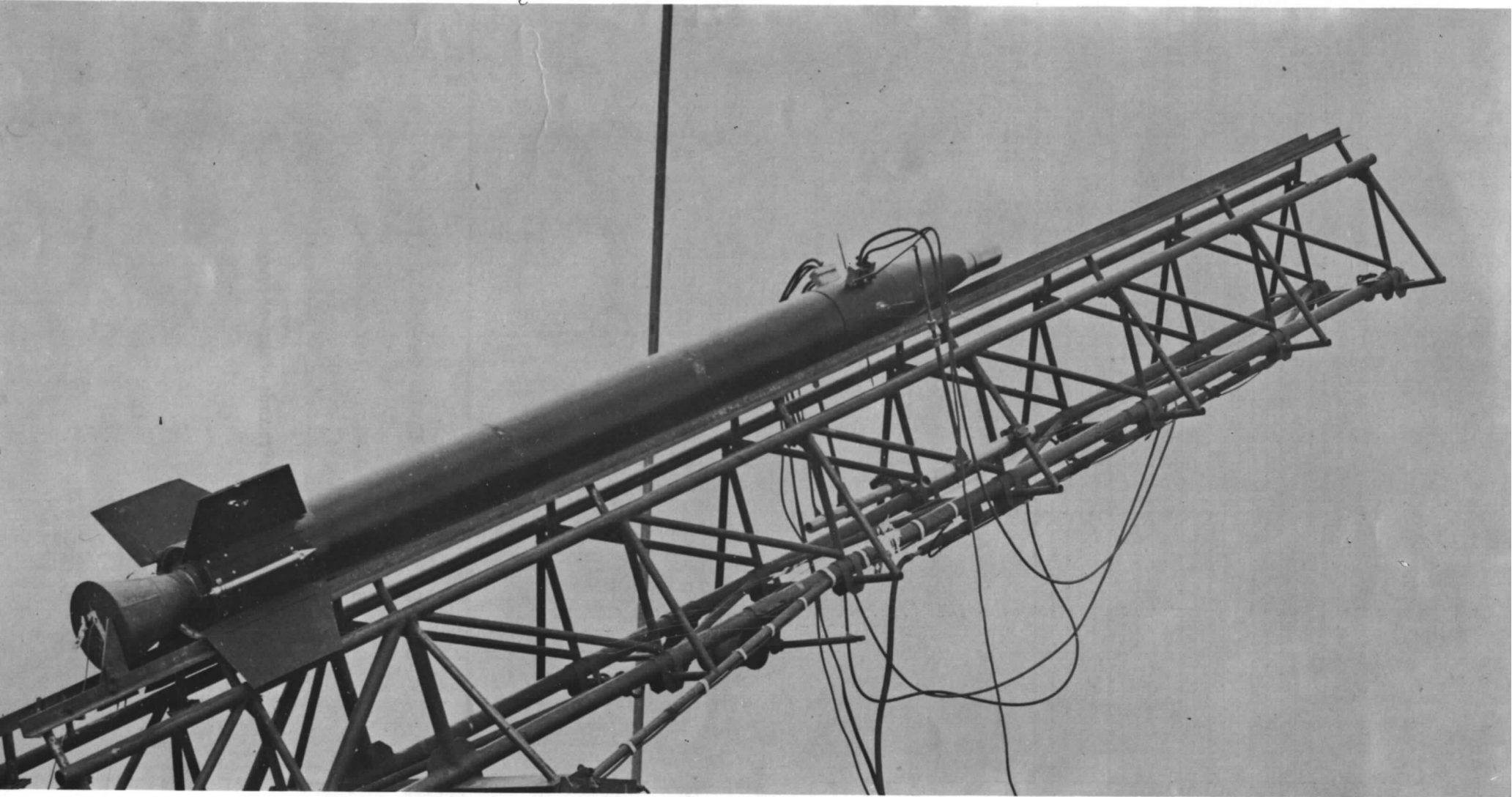
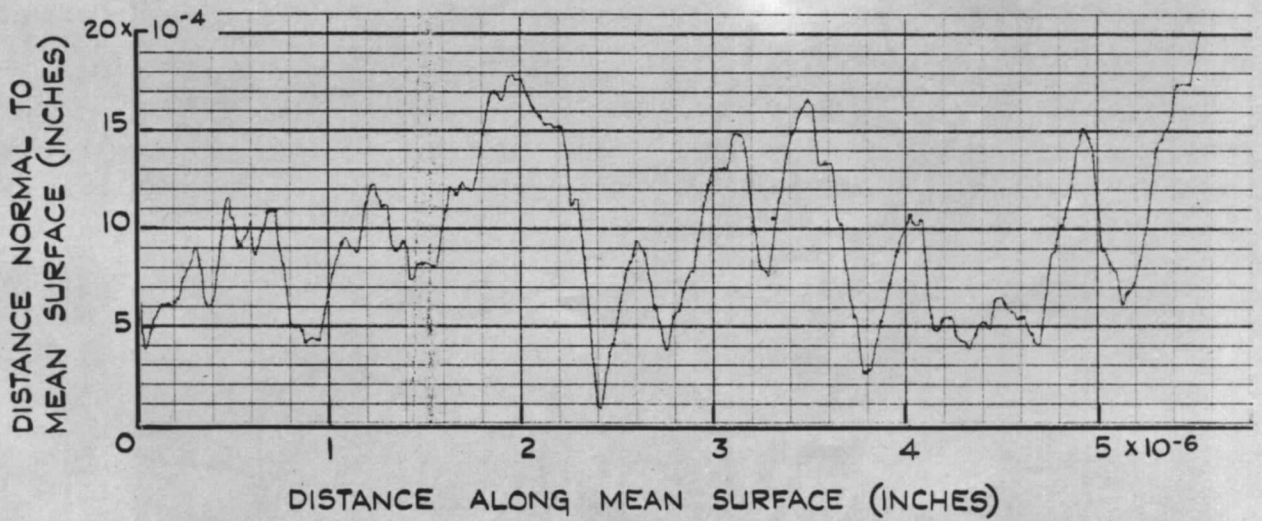
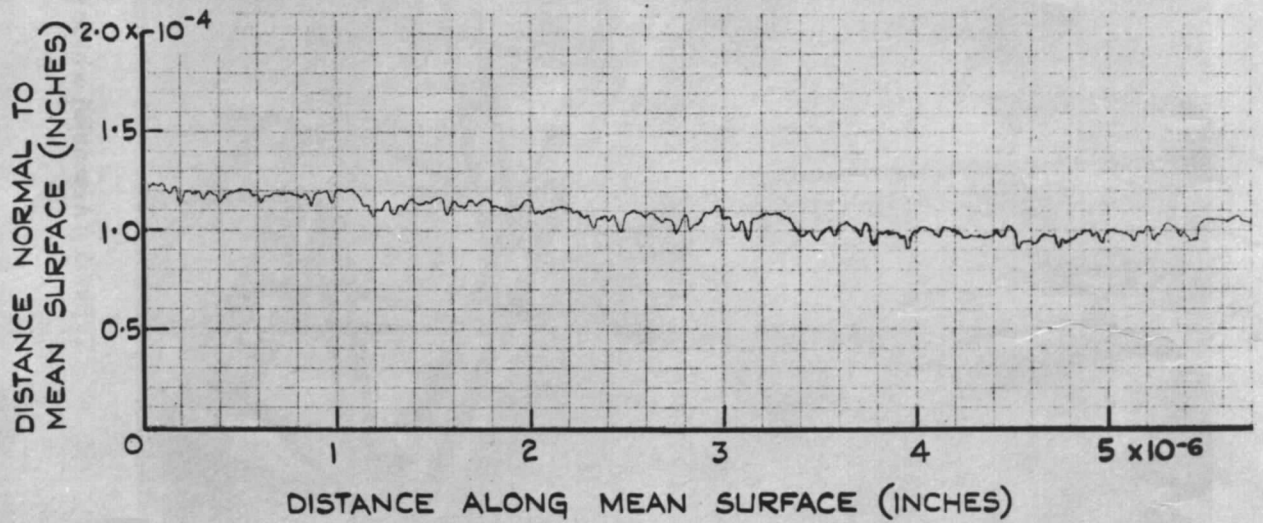


FIG. 5. Assembled vehicle prepared for flight.



ROUGH 10 inch HEMISPHERICAL HEAD (6)
 (C.L.A. $\doteq 200 \times 10^{-6}$ inches)



SMOOTH 10 inch HEMISPHERICAL HEAD (5)
 (C.L.A. $\doteq 3.5 \times 10^{-6}$ inches)

FIG. 6. Talysurf records of surface profiles.

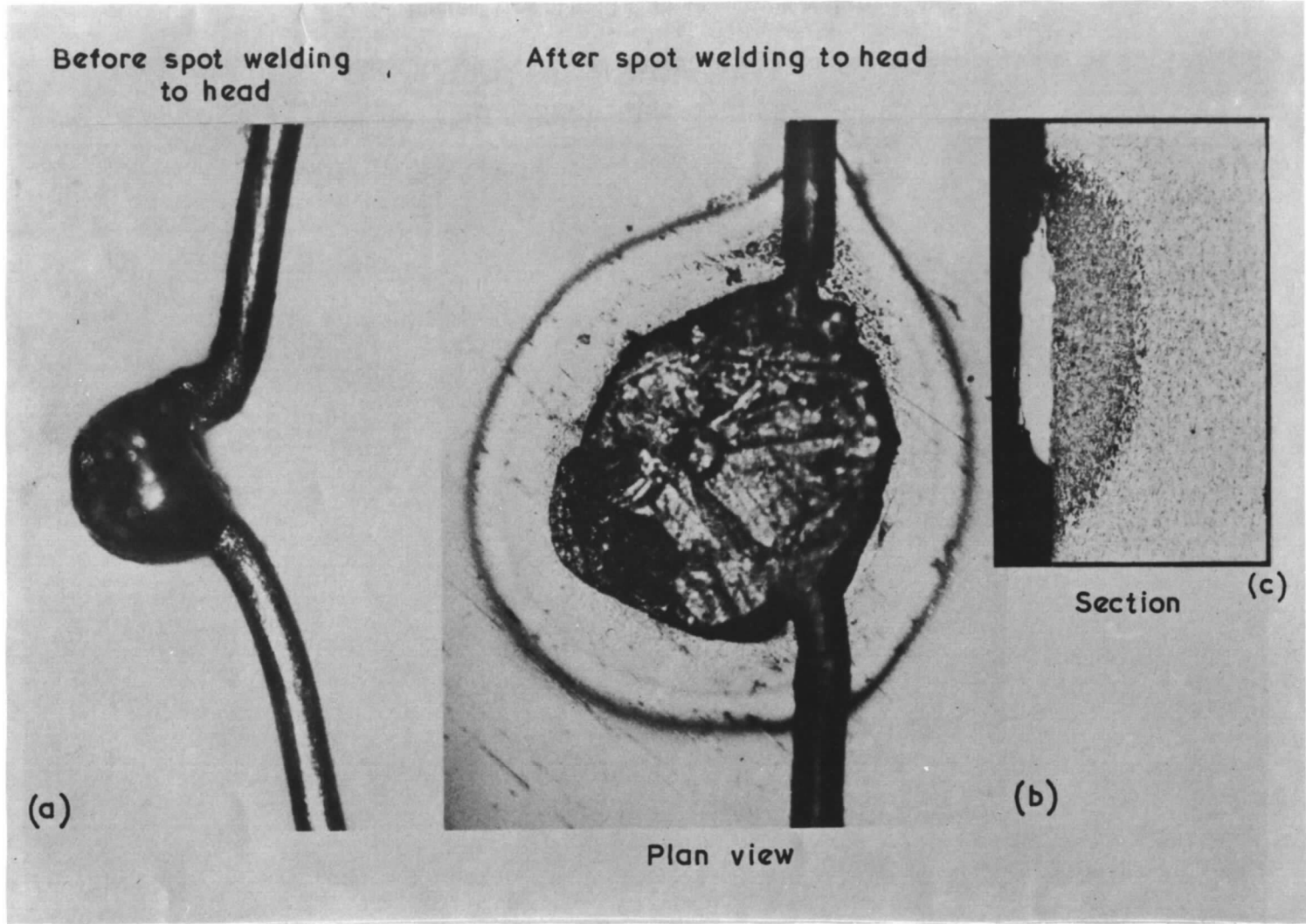


FIG. 7. Thermocouple weld (magnifications $\times 100$).

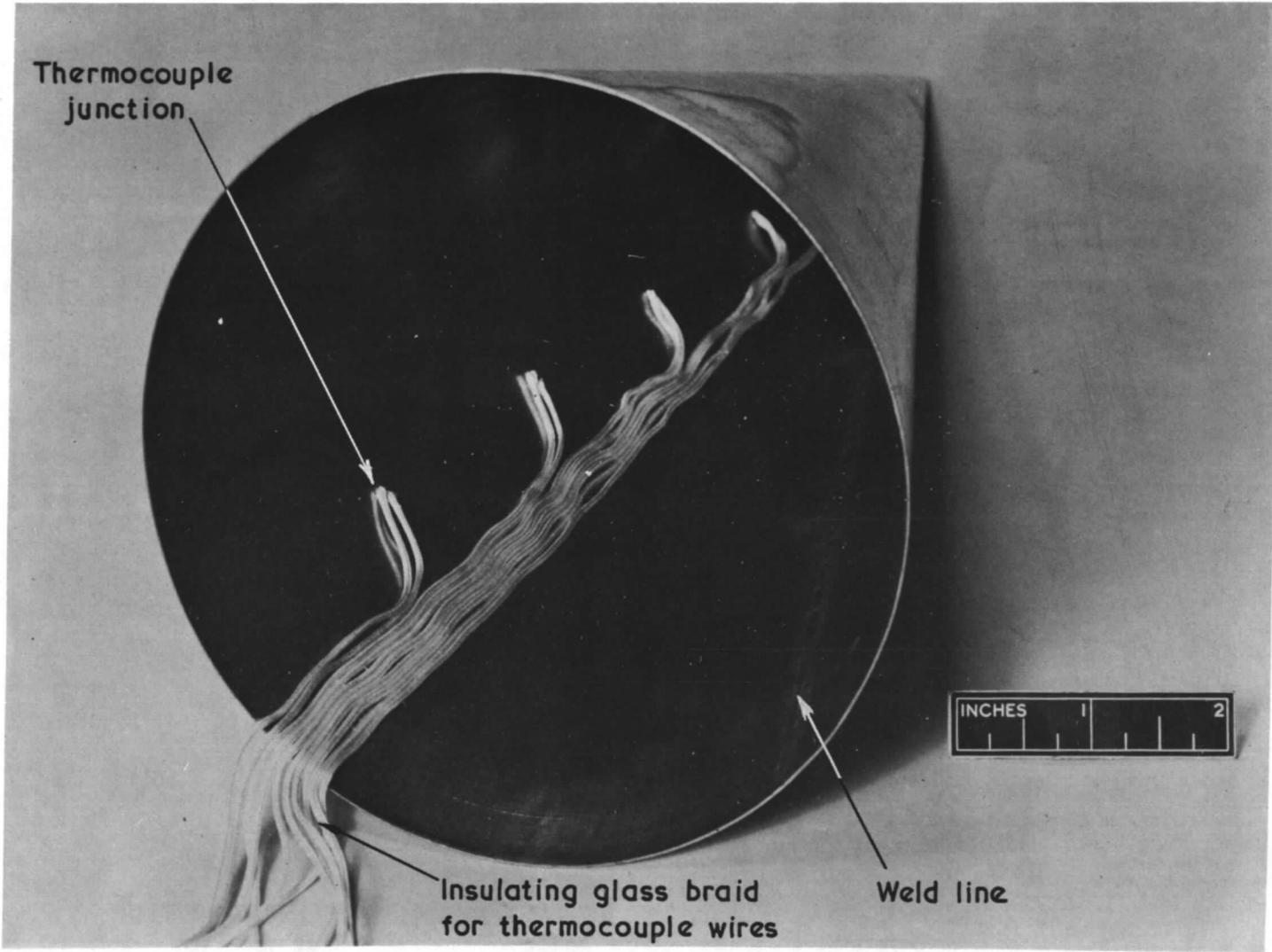
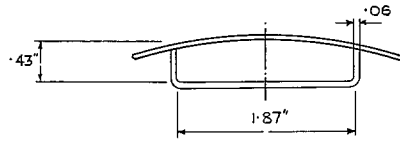


FIG. 8. Internal view of head showing location of thermocouples.



SECTION 'Y-Y' FULL SIZE.

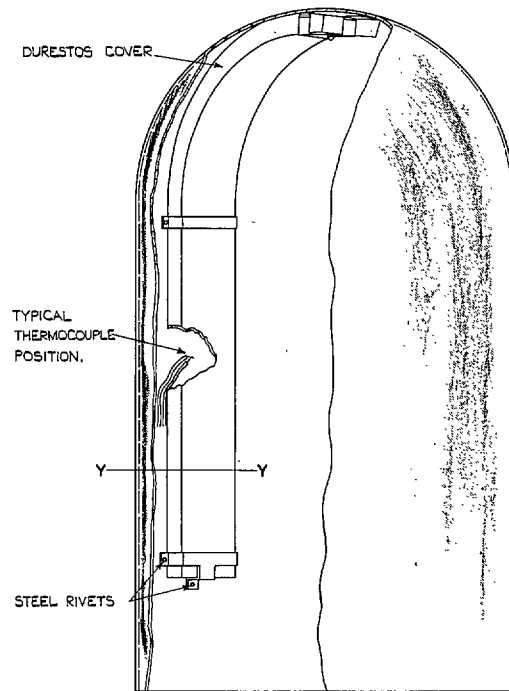


FIG. 9. Insulating durestos covers on 10 in. hemispheres.

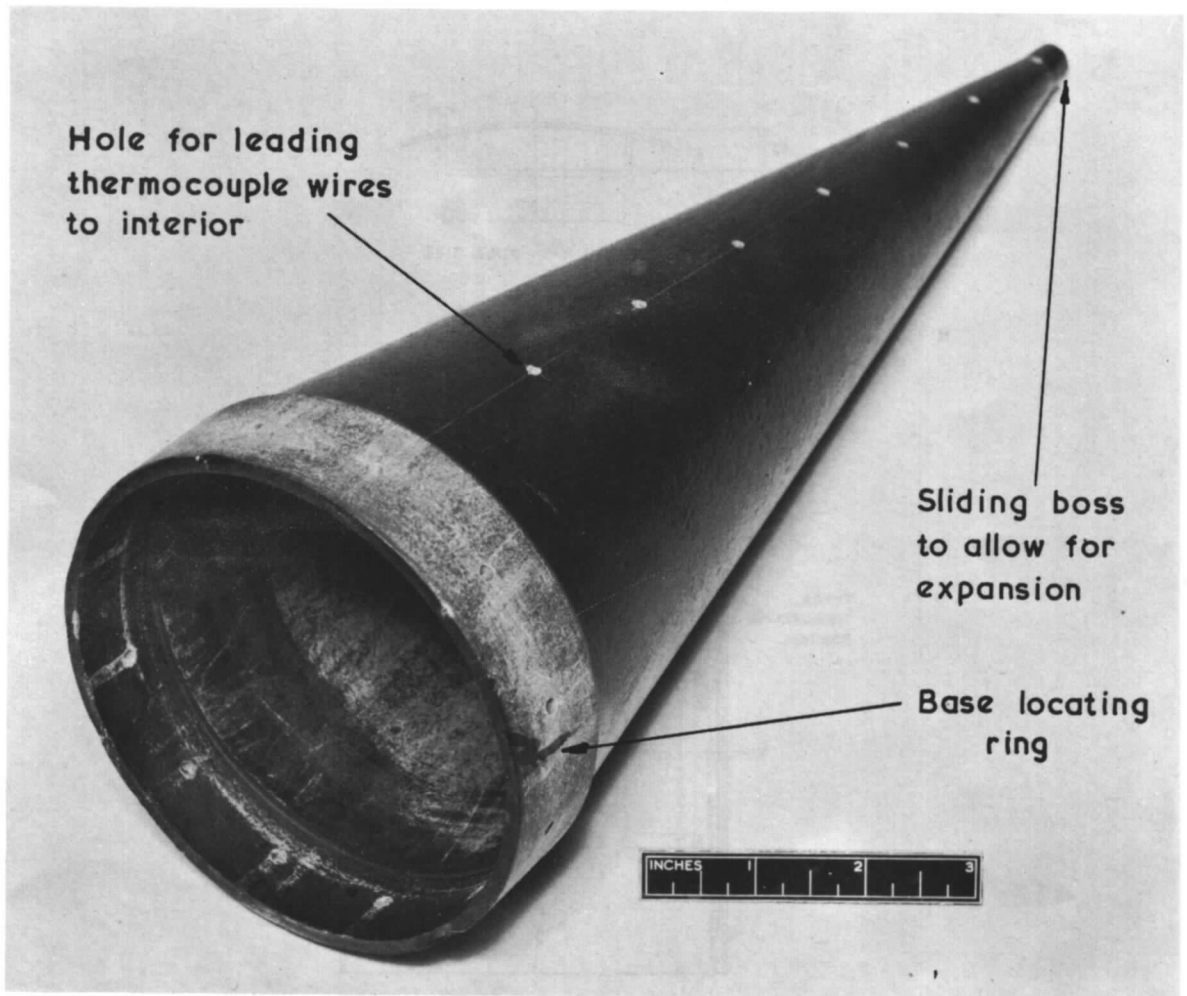


FIG. 10. Durestos inner wall.

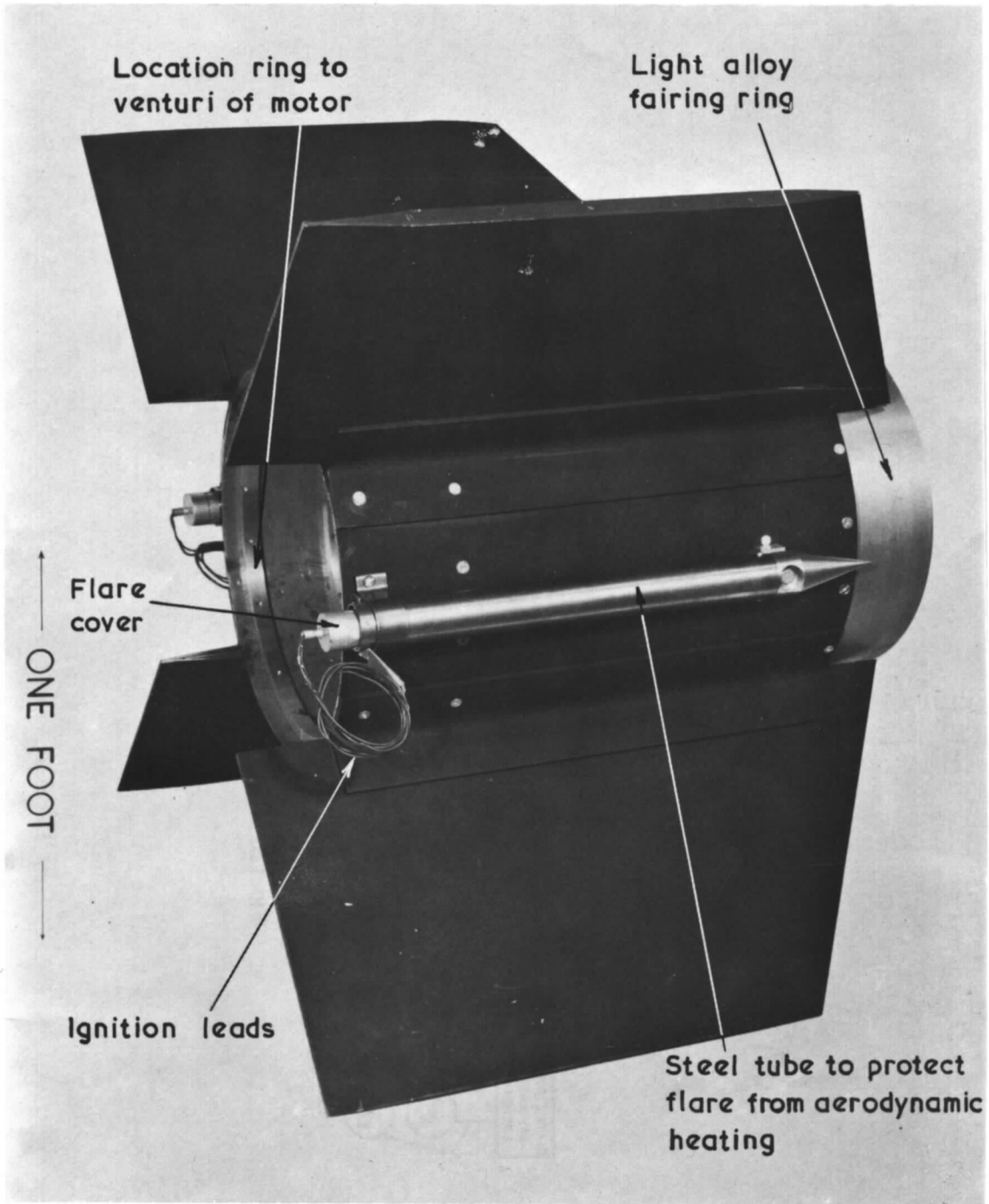


FIG. 11. Flares attached to fin assembly.

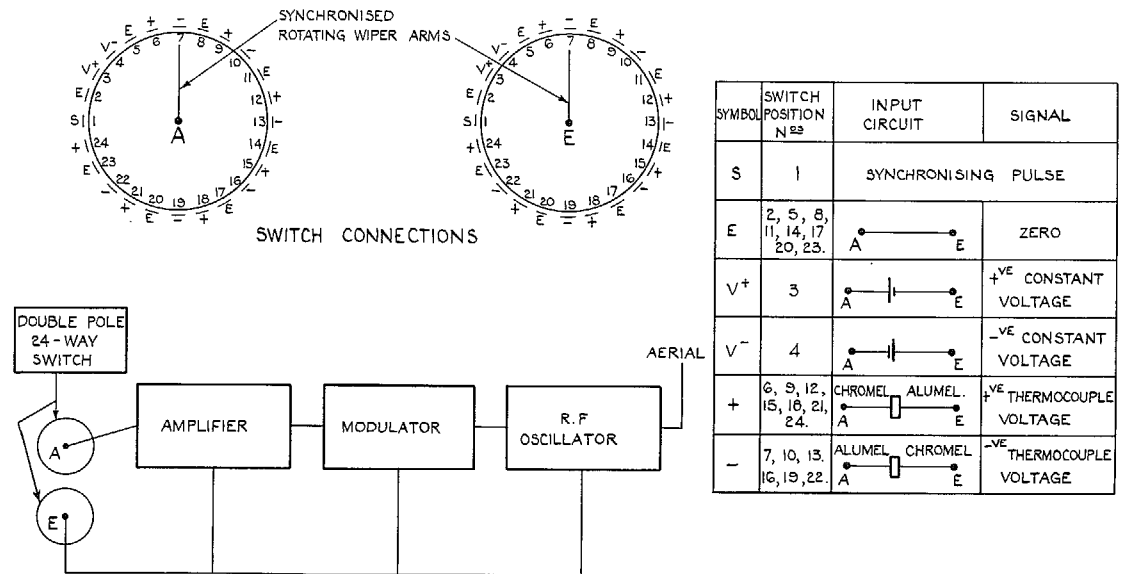


FIG. 12. Block diagram of telemetry equipment.

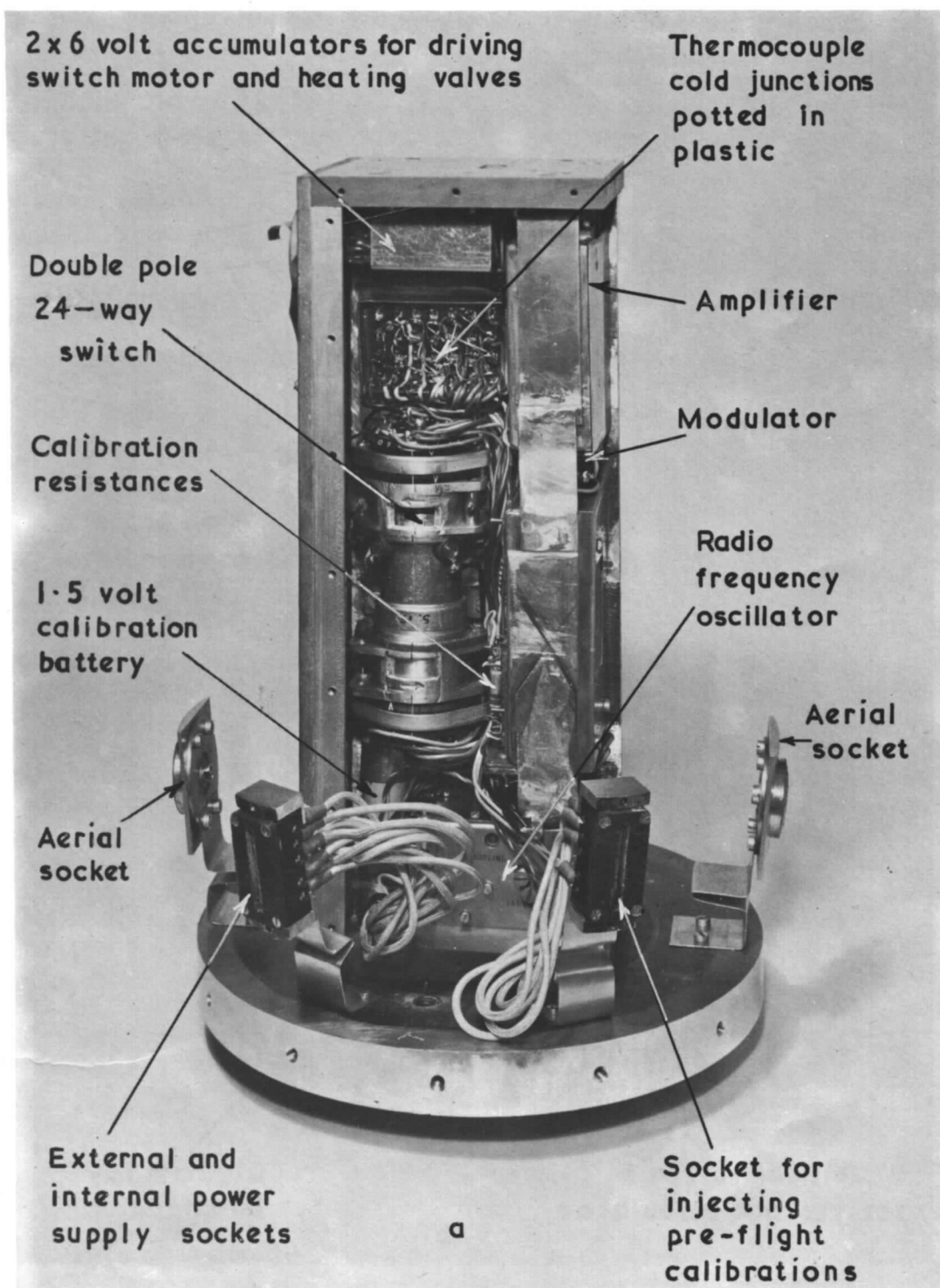


FIG. 13a. Telemetry unit.

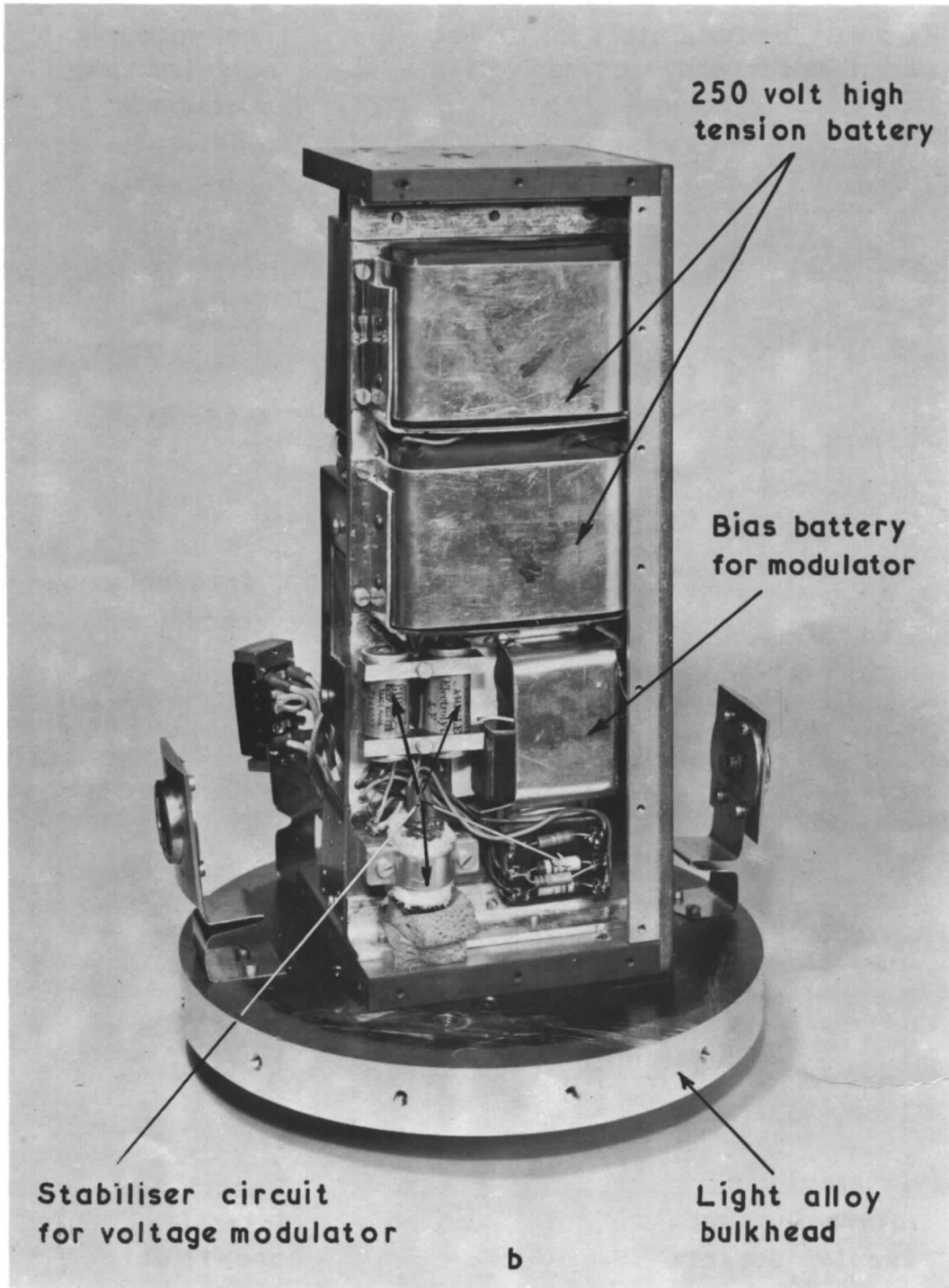


FIG. 13b. Telemetry unit.

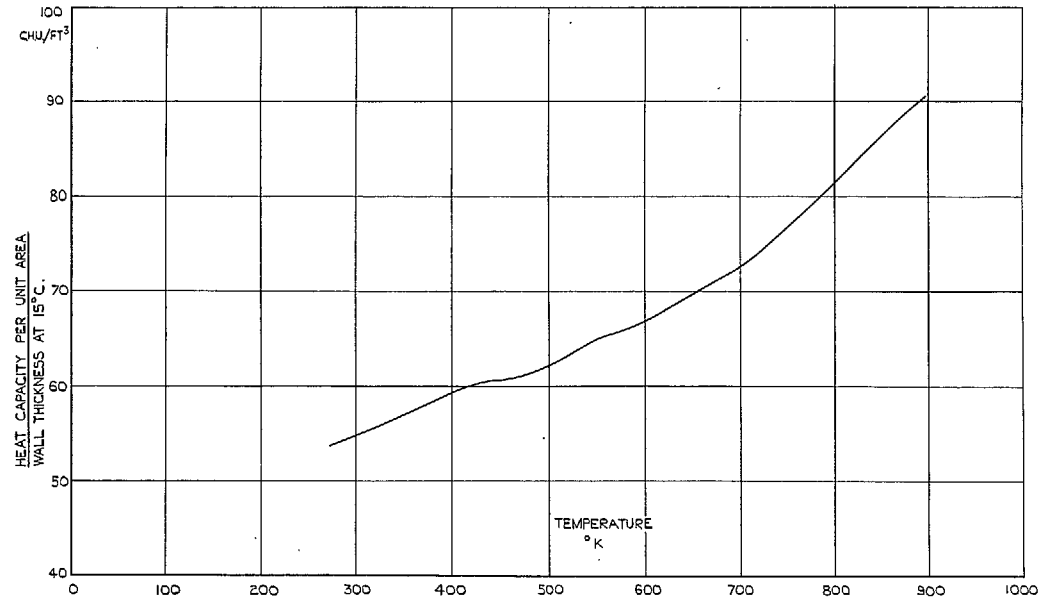
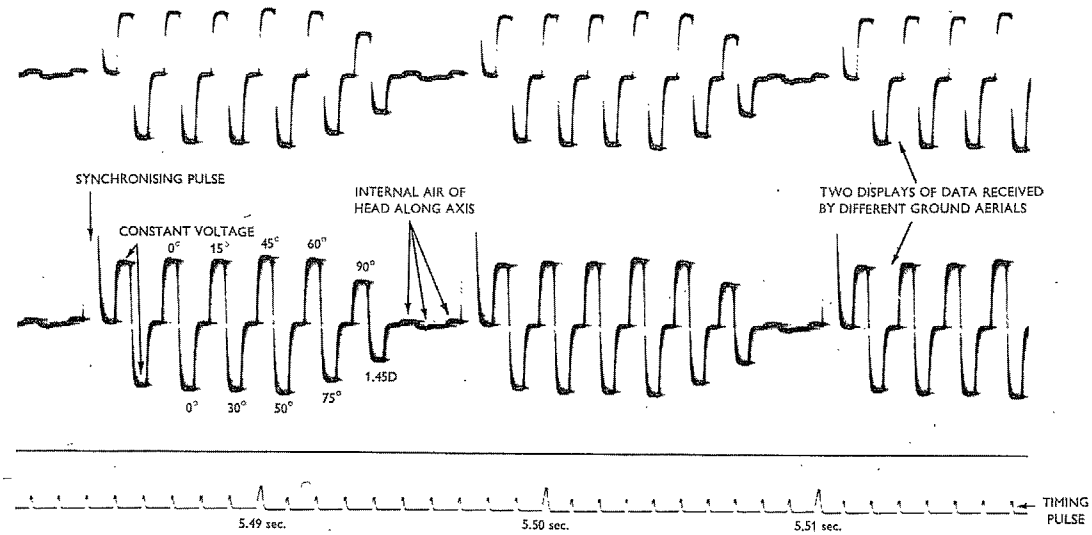


FIG. 14. Variation of heat capacity per unit area with temperature for mild steel.



THIS RECORD IS RELEVANT TO A HEMISPHERICAL HEAD. THE VARIOUS CHANNELS OF INFORMATION ARE IDENTIFIED FOR ONE CYCLE - THE WALL STATUSES BEING INDICATED BY THEIR ANGULAR CO-ORDINATES.

FIG. 15. Typical telemetry record.

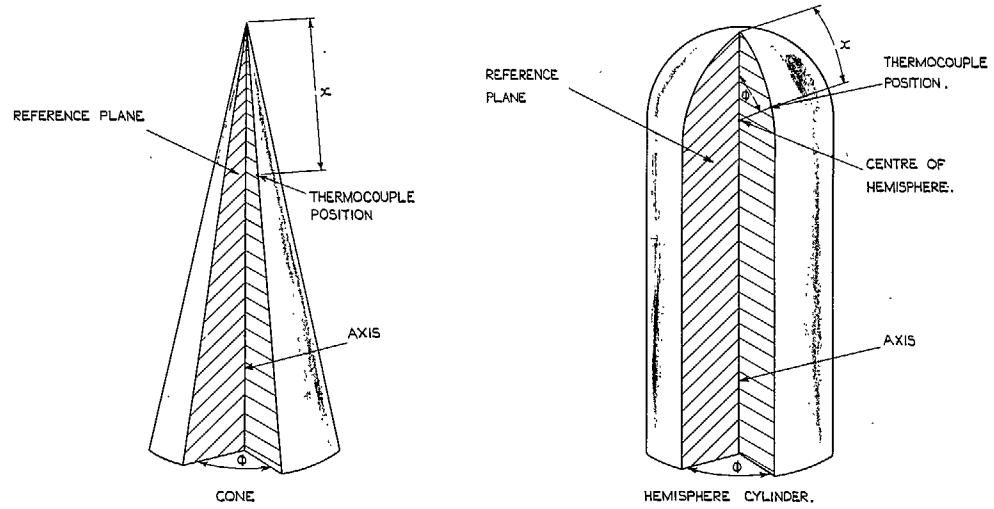


FIG. 16. System of head co-ordinates.

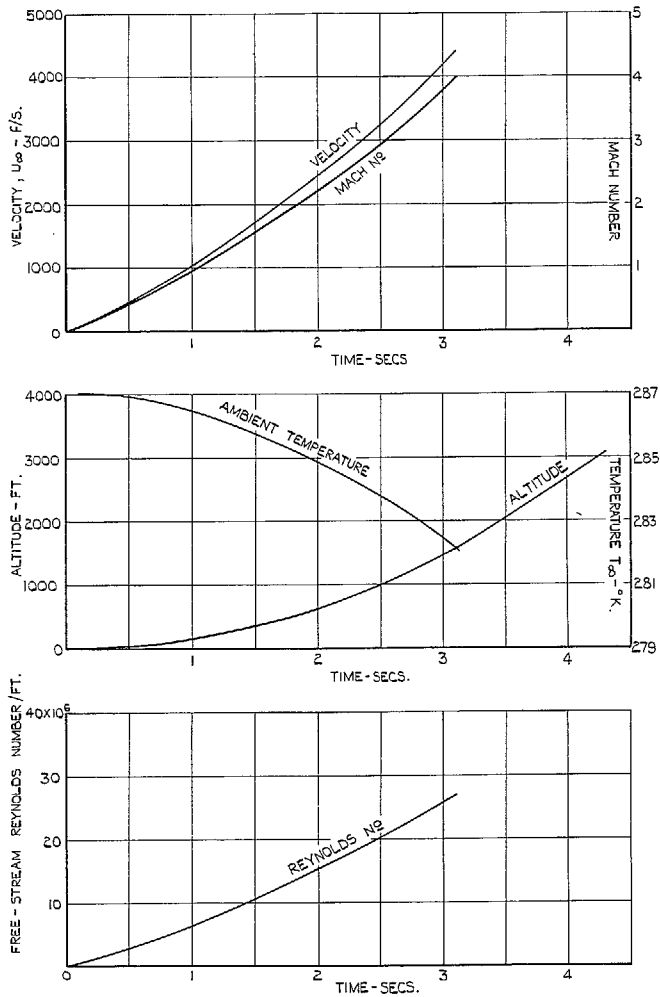


FIG. 17. Trajectory data for test vehicle 3 (smooth cone).

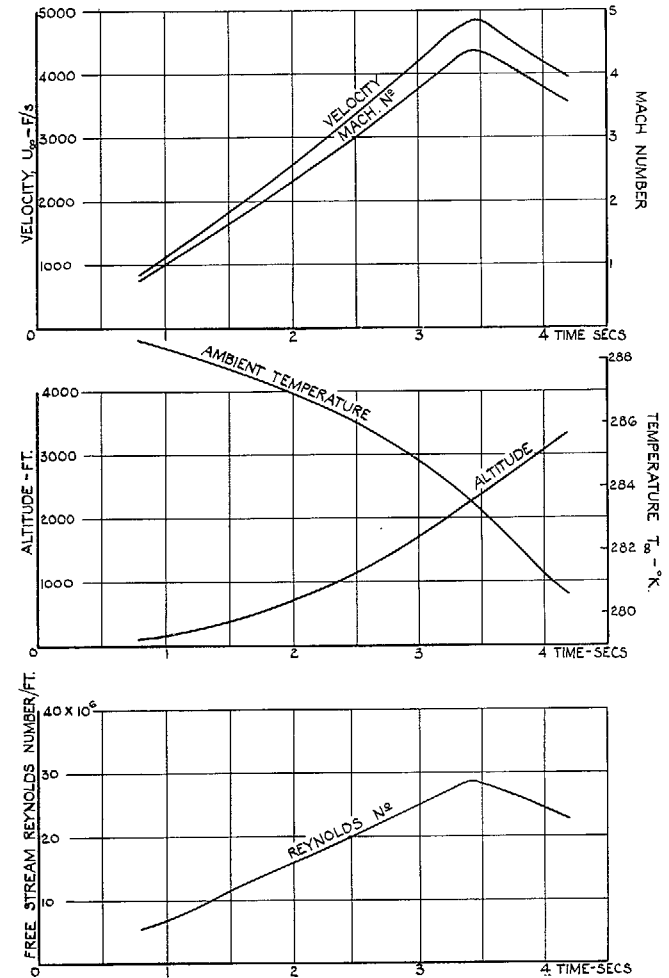


FIG. 18a. Trajectory data for 10 in. smooth hemisphere (head 5).

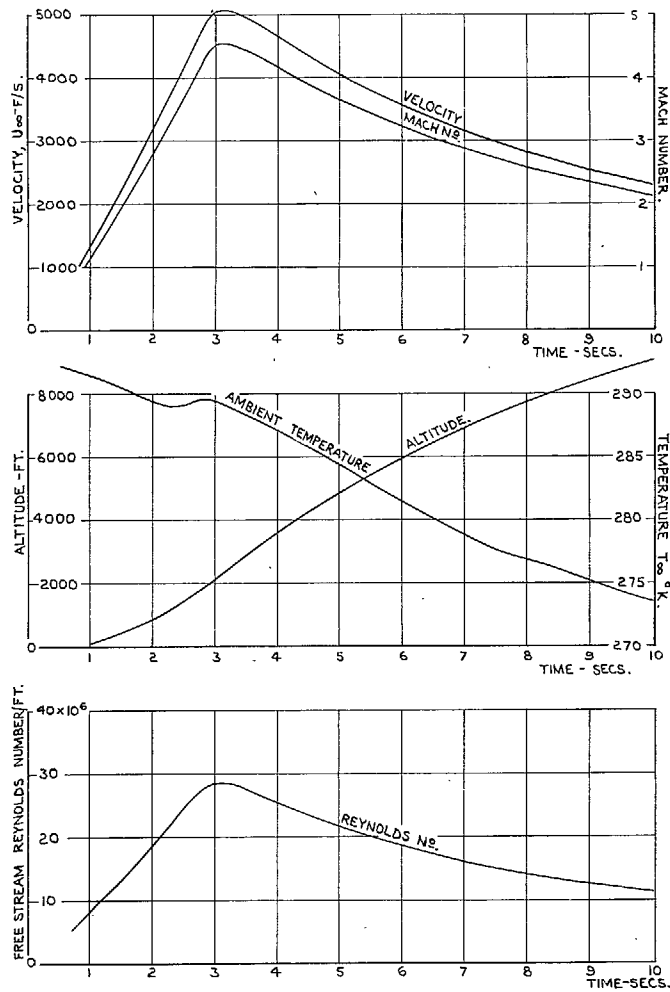


FIG. 18d. Trajectory data for 4 in. insulated hemisphere (head 9).

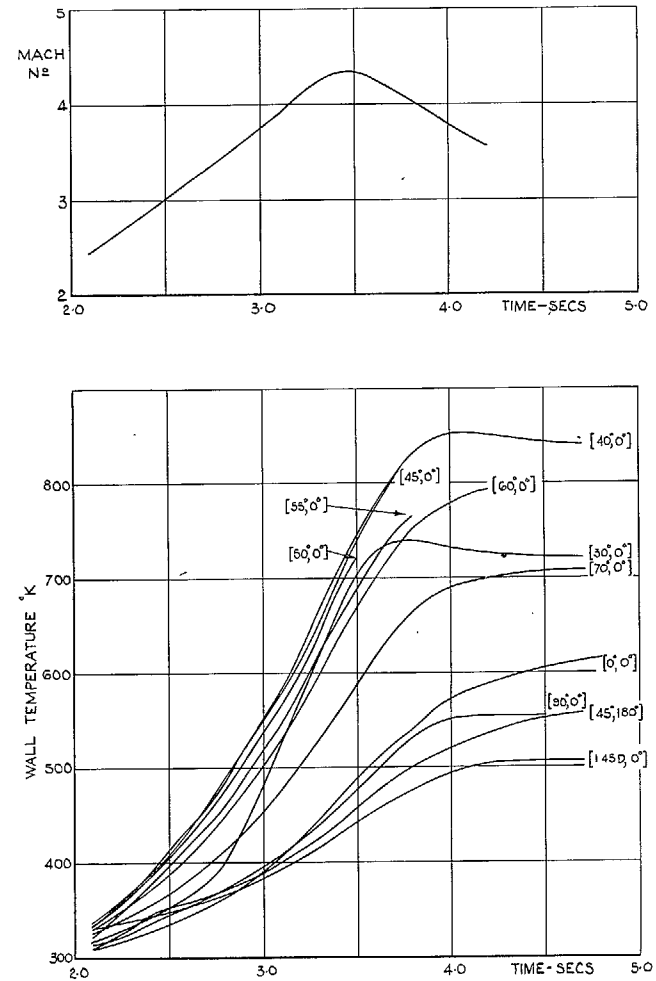


FIG. 19a. Variation of wall temperature with time for 10 in. smooth hemisphere (head 5).

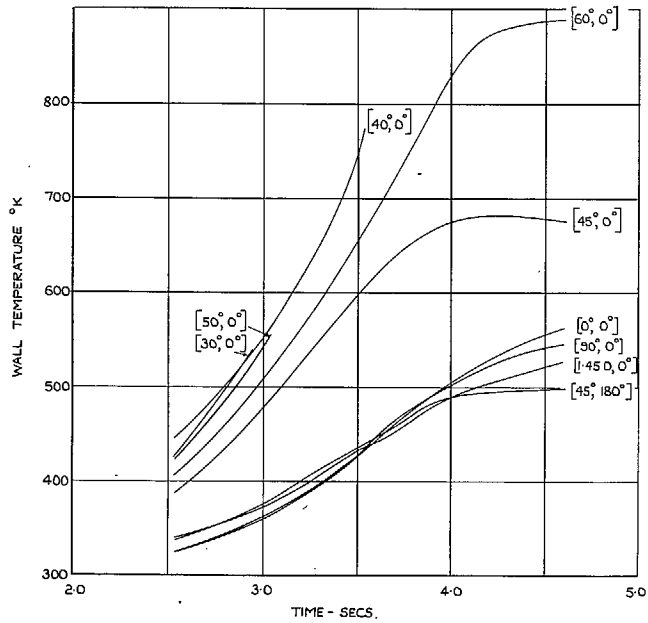
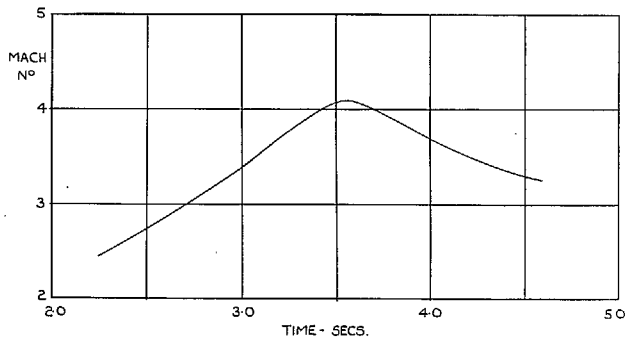


FIG. 19b. Variation of wall temperature with time for 10 in. rough hemisphere (head 6).

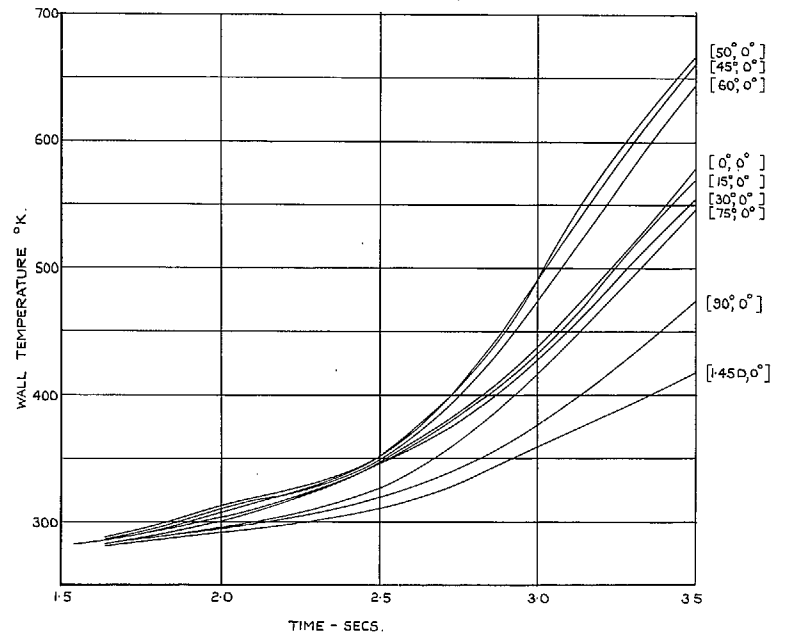
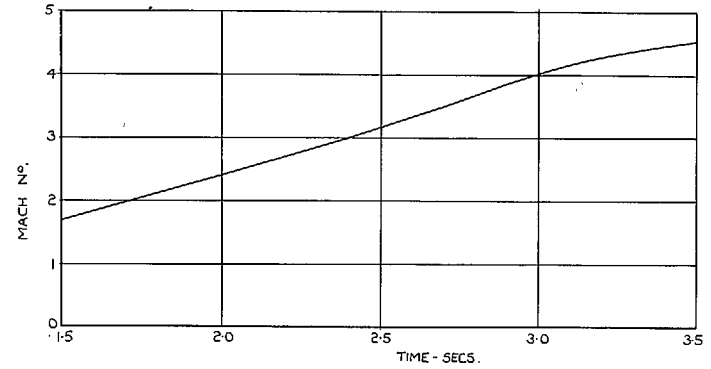


FIG. 19c. Variation of wall temperature with time for 4 in. hemisphere without internal insulation (head 8).

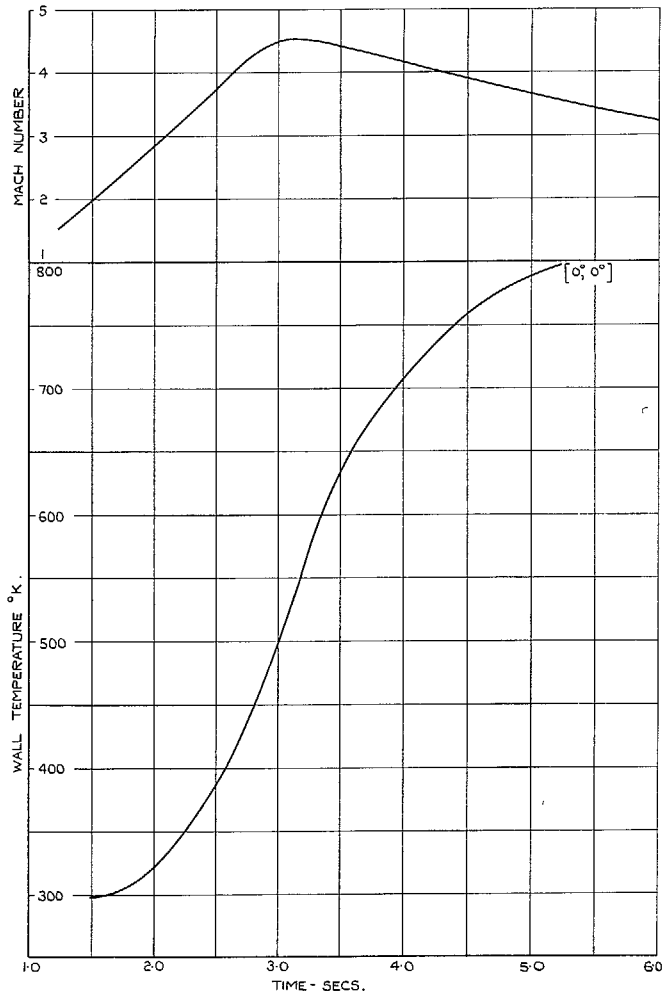


FIG. 19d. Variation of wall temperature with time for 4 in. insulated hemisphere (head 9).

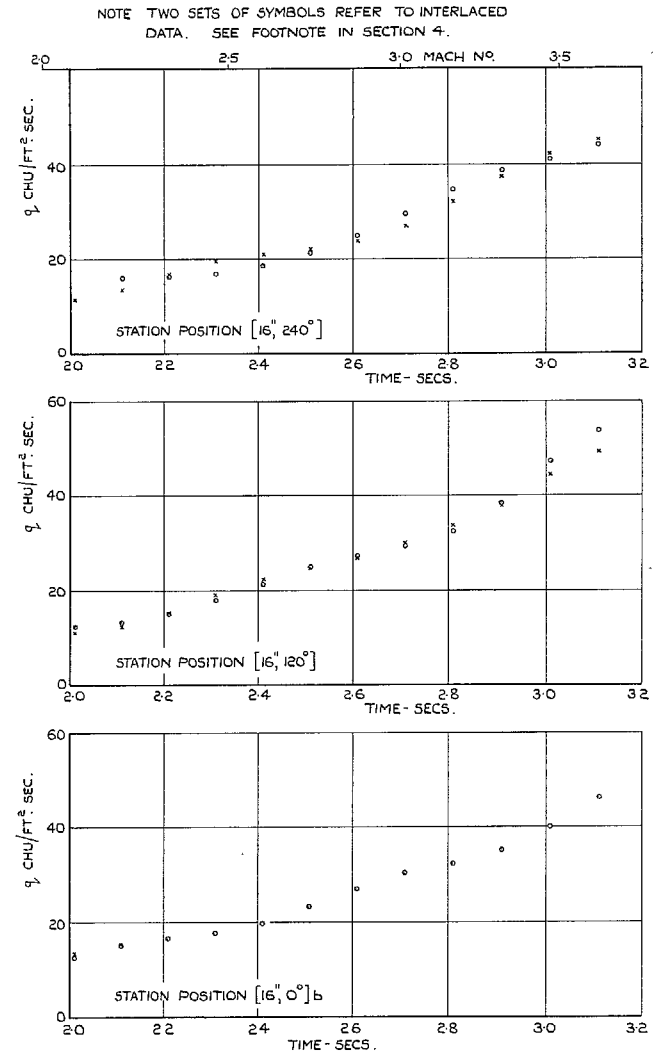
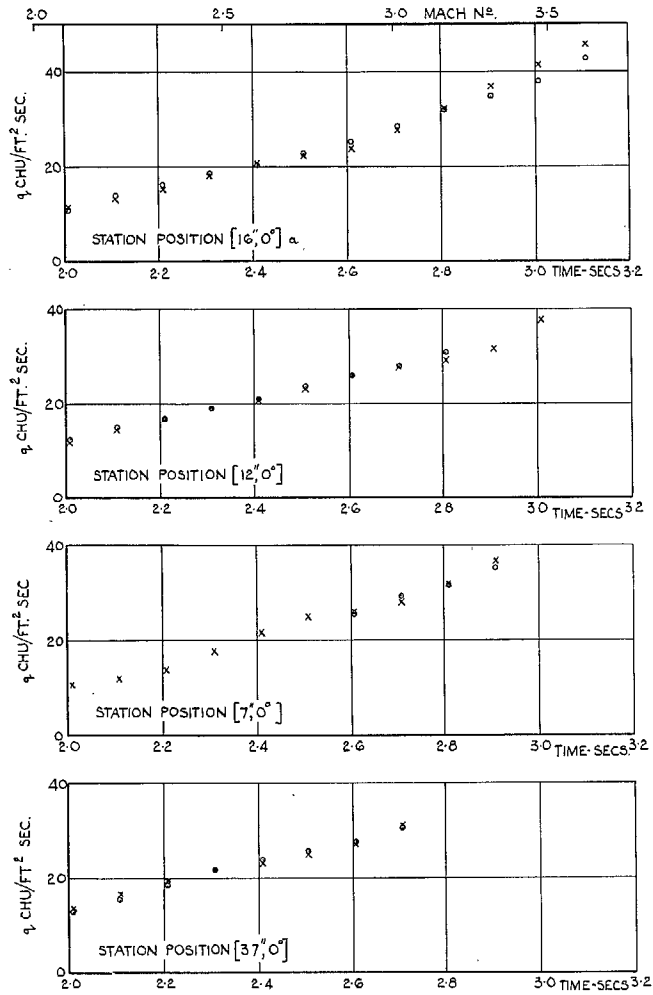
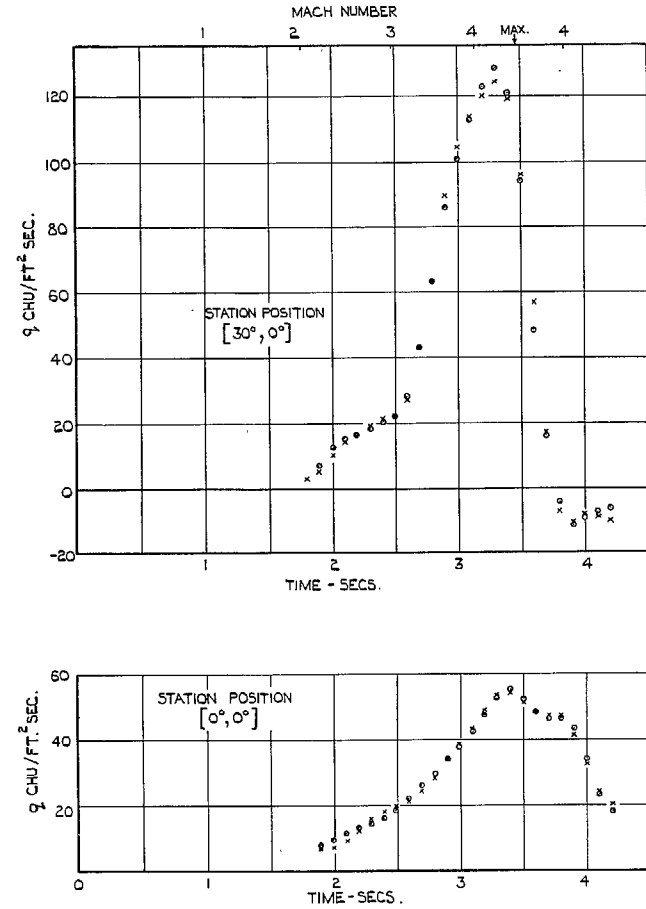


FIG. 20a. Local heat-transfer-rate histories for conical head 3.

NOTE. TWO SETS OF SYMBOLS REFER TO INTERLACED DATA.
SEE FOOTNOTE IN SECTION 4.



NOTE:~ TWO SETS OF SYMBOLS REFER TO INTERLACED DATA. SEE FOOTNOTE IN SECTION 4.



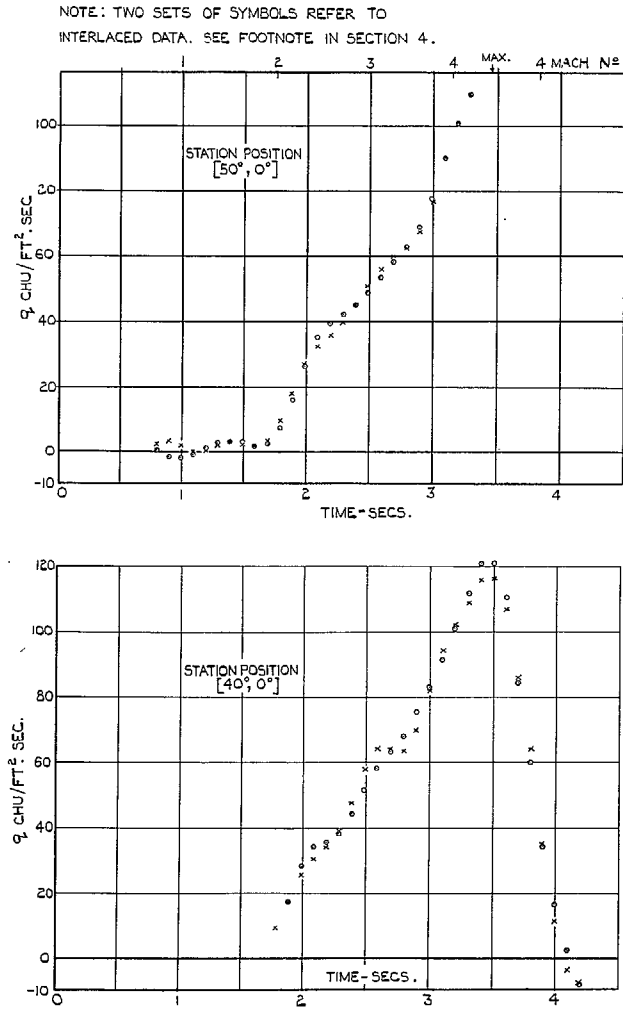


FIG. 20b (contd.). Local heat-transfer histories for head 5—stations [40°, 0°] and [50°, 0°].

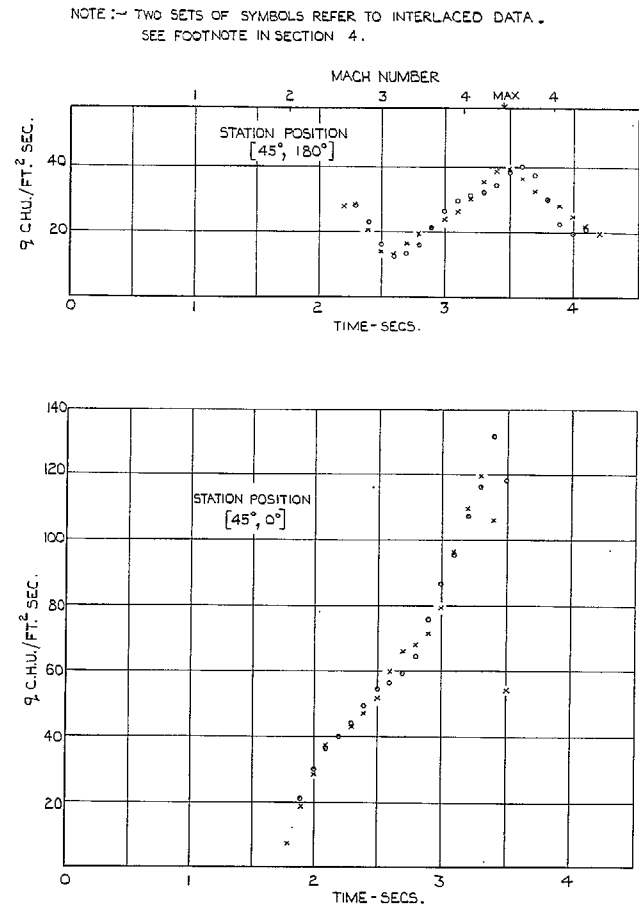


FIG. 20b (contd.). Local heat-transfer histories for head 5—stations [45°, 0°] and [45°, 180°].

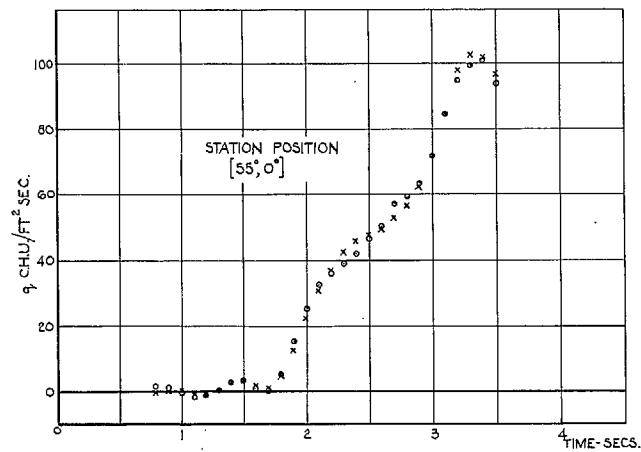
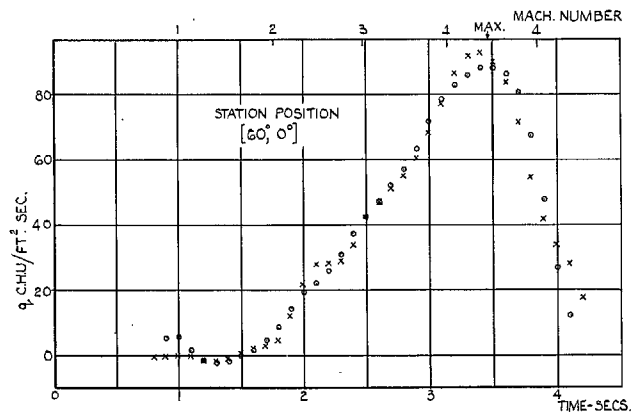


FIG. 20b (contd.). Local heat-transfer histories for head 5—stations [55°, 0°] and [60°, 0°].

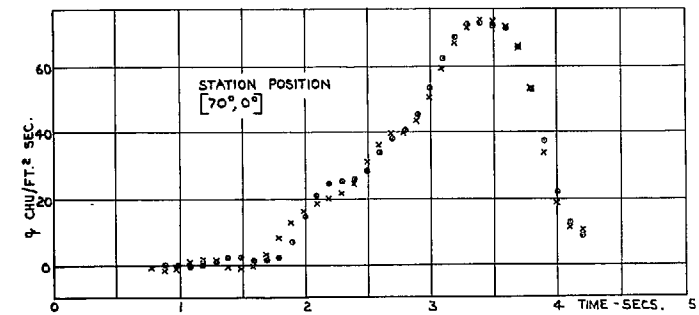
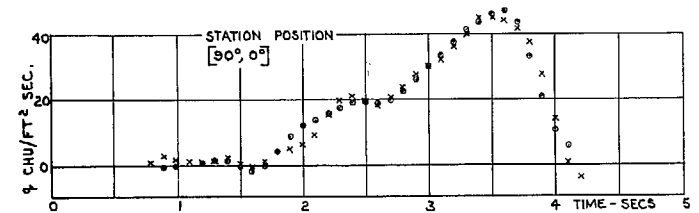
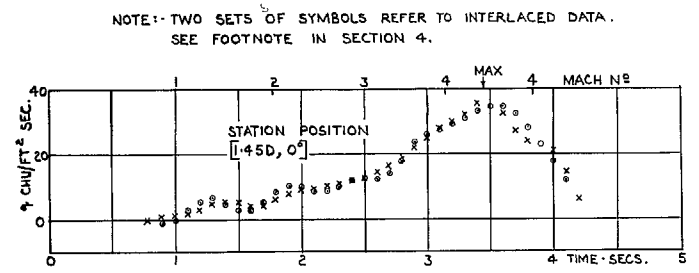


FIG. 20b (contd.). Local heat-transfer histories for head 5—stations [70°, 0°], [90°, 0°] & [1.45D, 0°].

NOTE: TWO SETS OF SYMBOLS REFER TO INTERLACED DATA.
SEE FOOTNOTE IN SECTION 4.

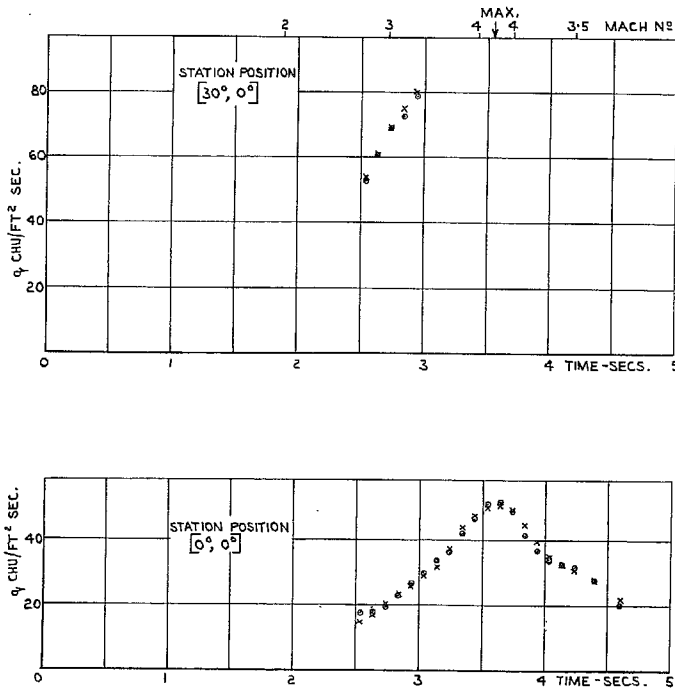


FIG. 20c. Local heat-transfer histories for head 6-stations $[0^\circ, 0^\circ]$ & $[30^\circ, 0^\circ]$.

NOTE:- TWO SETS OF SYMBOLS REFER TO INTERLACED DATA.
SEE FOOTNOTE IN SECTION 4.

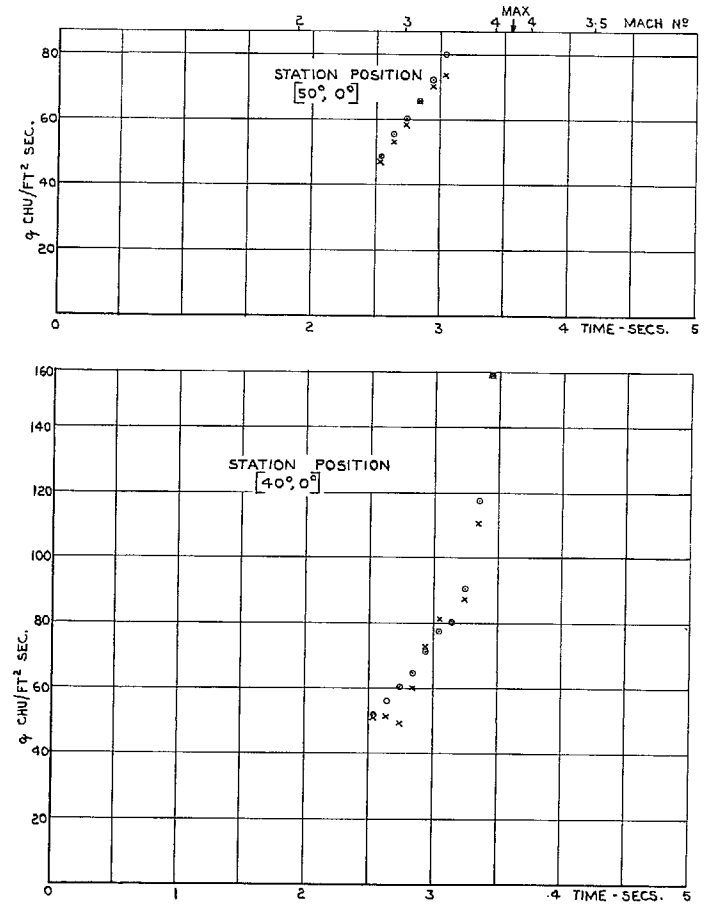


FIG. 20c (contd.). Local heat-transfer histories for head 6-stations $[40^\circ, 0^\circ]$ & $[50^\circ, 0^\circ]$.

NOTE:- TWO SETS OF SYMBOLS REFER TO INTERLACED DATA.
SEE FOOTNOTE IN SECTION 4.

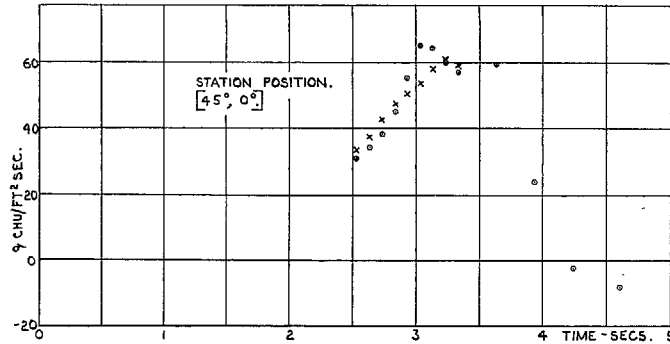
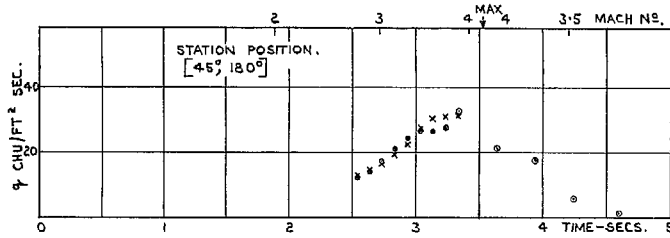


FIG. 20c (contd.). Local heat-transfer histories for head 6—stations $[45^\circ, 0^\circ]$ & $[45^\circ, 180^\circ]$.

NOTE TWO SETS OF SYMBOLS REFER TO INTERLACED DATA
SEE FOOTNOTE IN SECTION 4.

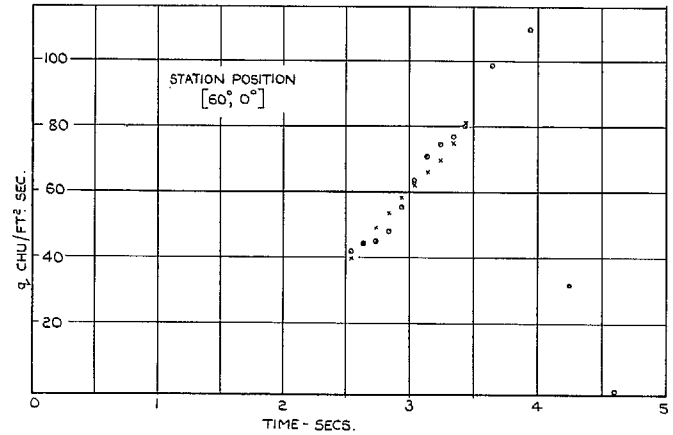
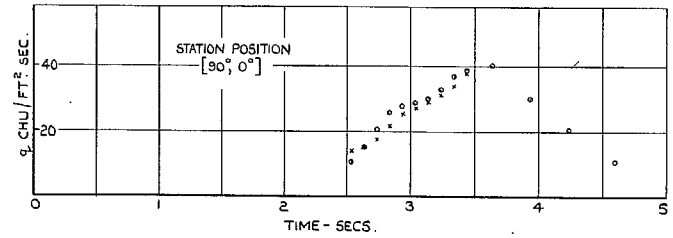
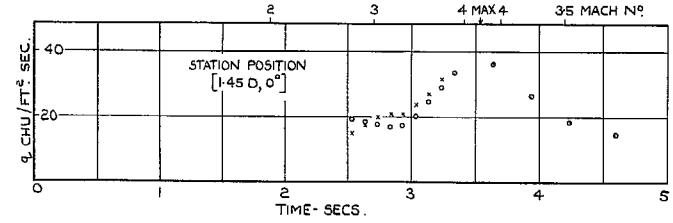


FIG. 20c (contd.). Local heat-transfer histories for head 6—stations $[60^\circ, 0^\circ]$, $[90^\circ, 0^\circ]$ and $[1.45D, 0^\circ]$.

NOTE: TWO SETS OF SYMBOLS REFER TO INTERLACED DATA.
SEE FOOTNOTE IN SECTION 4.

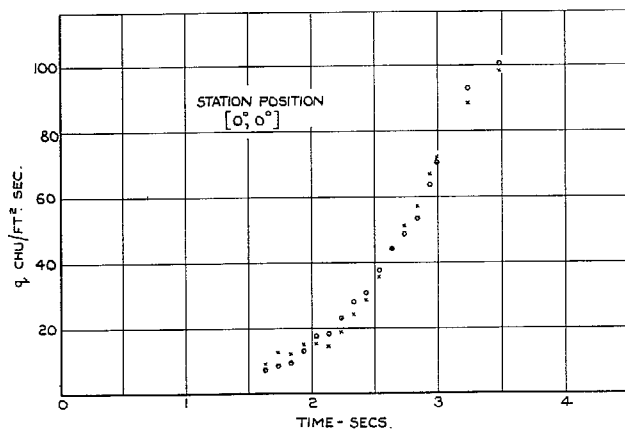
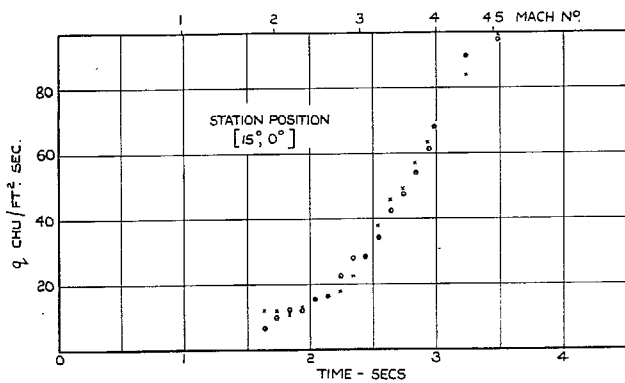


FIG. 20d. Local heat-transfer histories for head 8-stations $[0^\circ, 0^\circ]$ and $[15^\circ, 0^\circ]$.

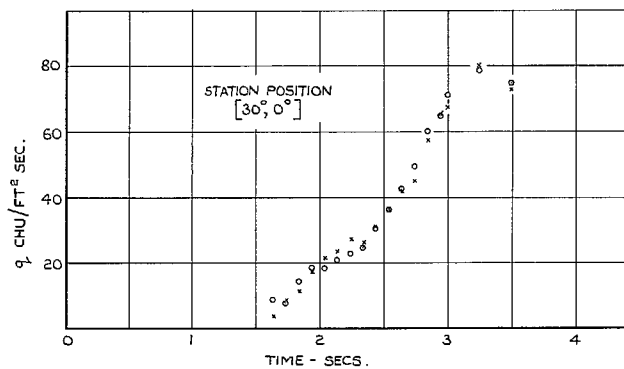
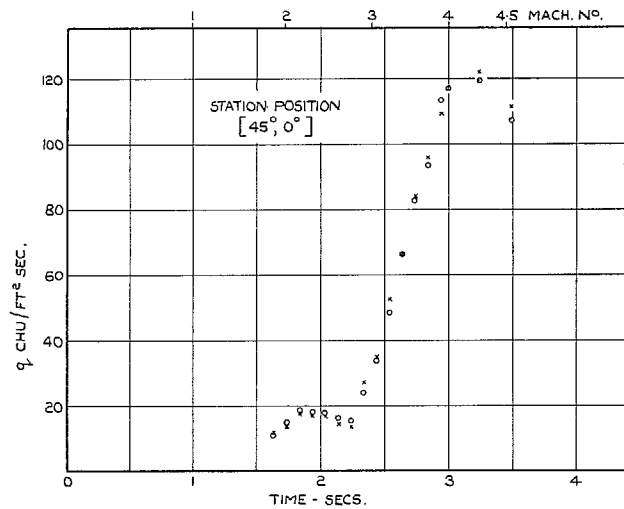


FIG. 20d (contd.). Local heat-transfer histories for head 8-stations $[30^\circ, 0^\circ]$ and $[45^\circ, 0^\circ]$.

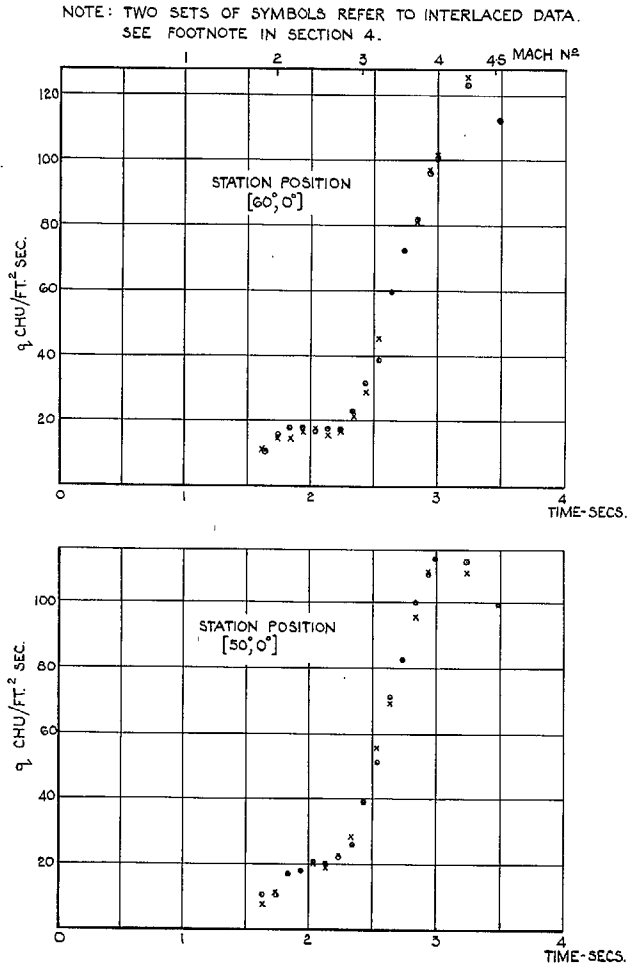


FIG. 20d (contd.). Local heat-transfer histories for head 8—stations [50°, 0°] and [60°, 0°].

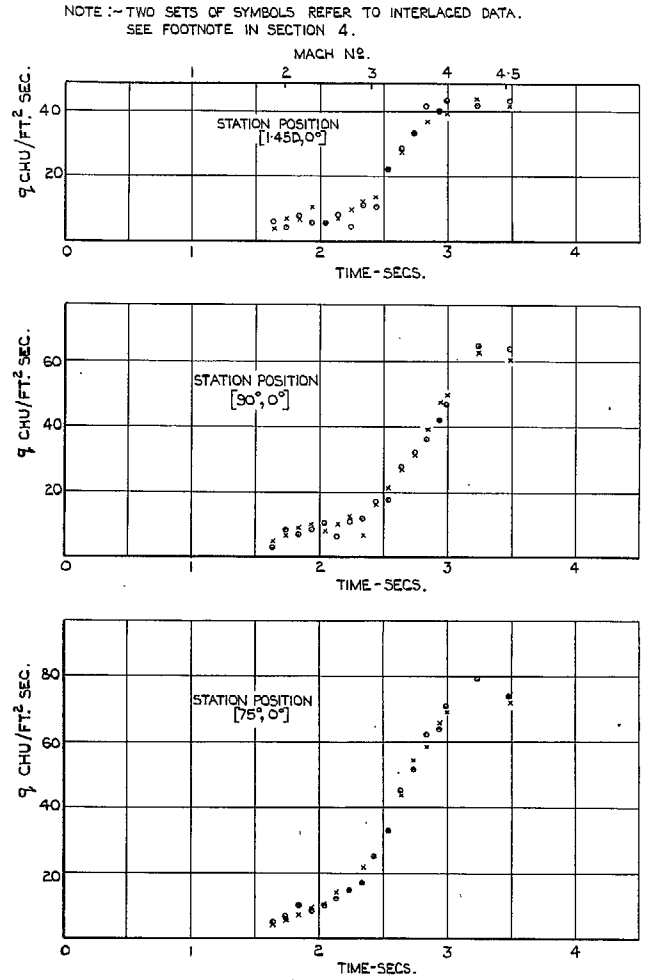


FIG. 20d (contd.). Local heat-transfer histories for head 8—stations [75°, 0°], [90°, 0°] and [1.45D, 0°].

NOTE: TWO SETS OF SYMBOLS REFER TO INTERLACED DATA.
SEE FOOTNOTE IN SECTION 4.

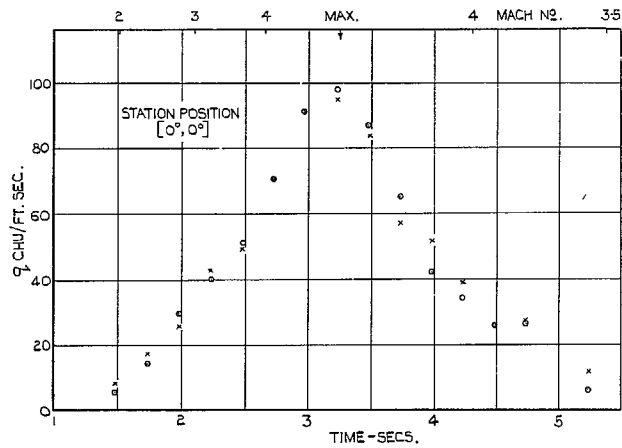


FIG. 20e. Local heat-transfer histories for head 9—station [0°, 0°].

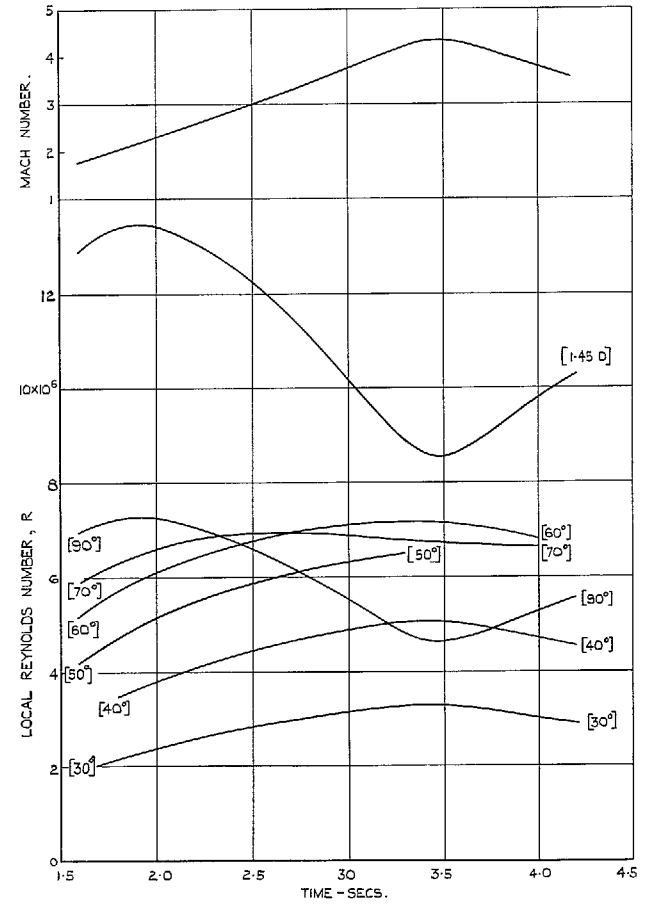


FIG. 21. Variation of local Reynolds number, R , with time for the stations on the hemispherical head 5.

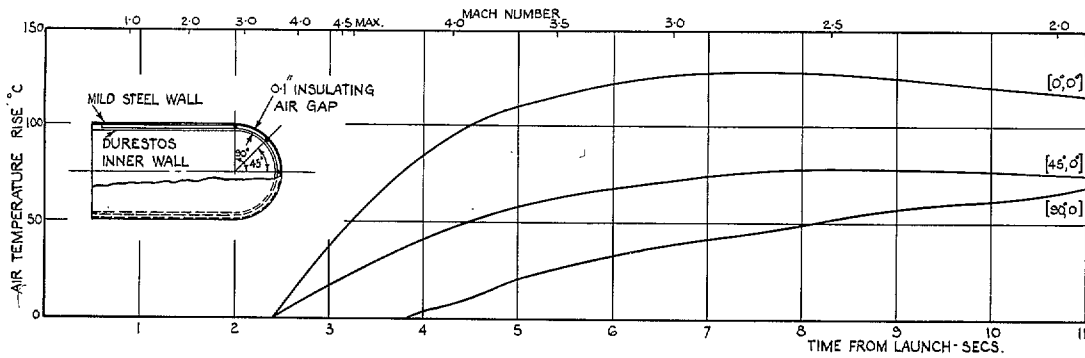


FIG. 22a. Temperature histories of insulating air gap in 4 in. hemisphere (head 9).

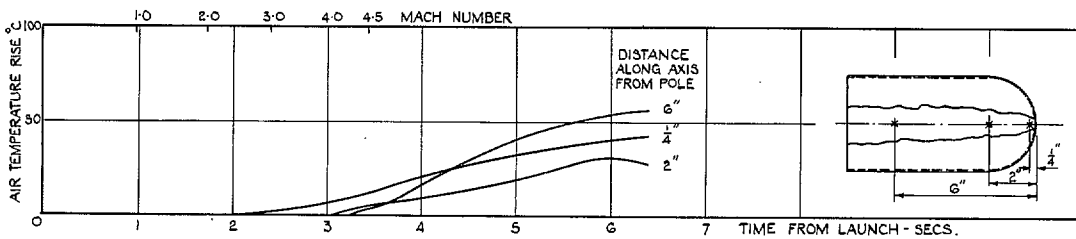


FIG. 22b. Temperature histories of air along axis of uninsulated 4 in. hemisphere (head 8).

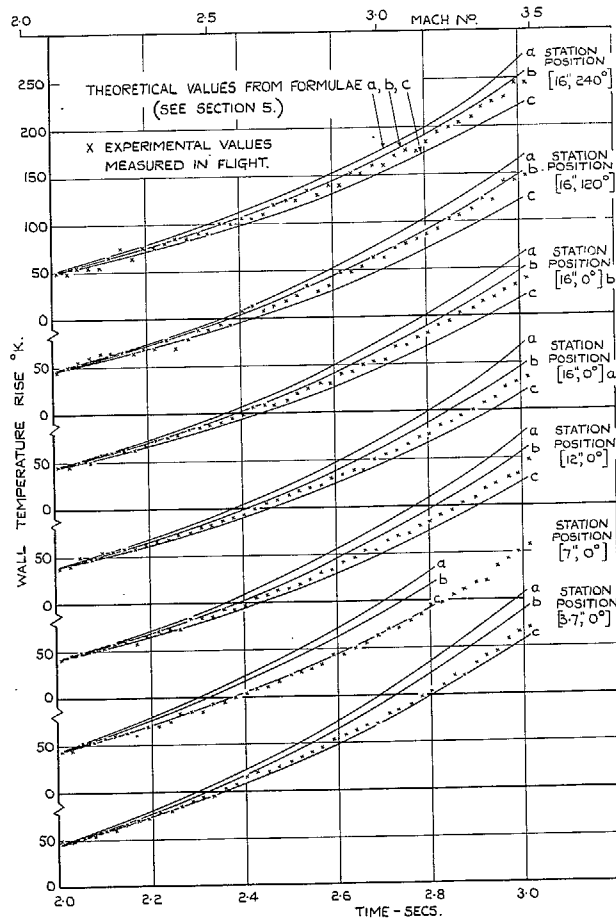


FIG. 23. Comparison of temperature measurements with theory for conical head 3.

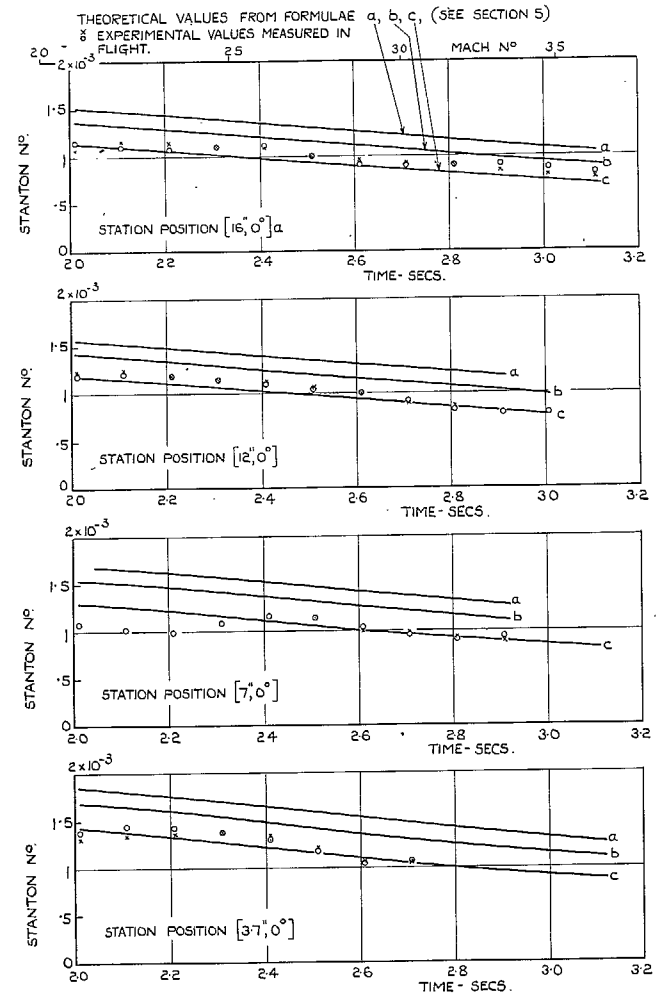


FIG. 24a. Comparison of experimental Stanton numbers with theory for conical head 3.

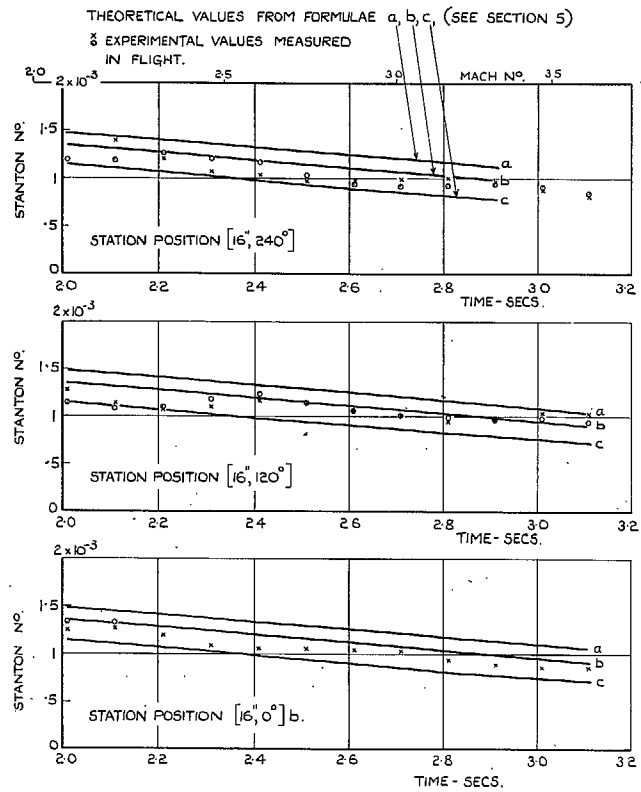


FIG. 24b. Comparison of experimental Stanton numbers with theory for conical head 3.

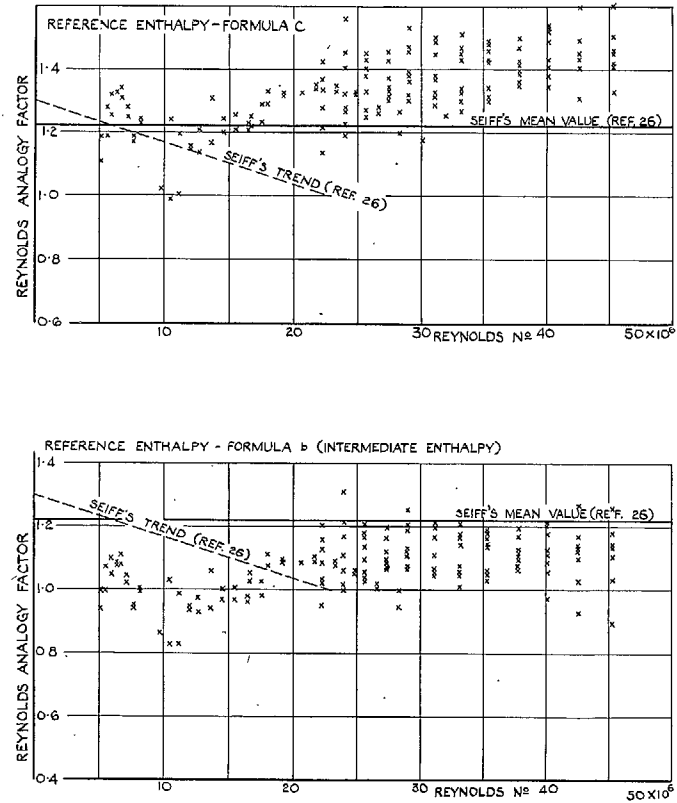


FIG. 25. Variation of Reynolds' analogy factor with Reynolds number for cone for two reference enthalpies.

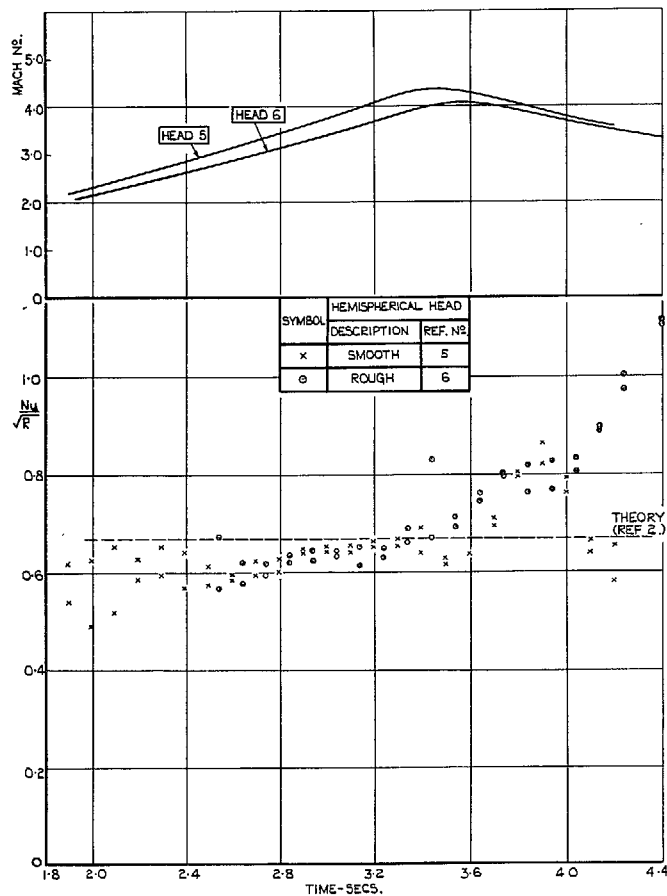


FIG. 26a. Variation of Nu/\sqrt{R} with time and Mach number for 10 in. hemispheres at stagnation point.

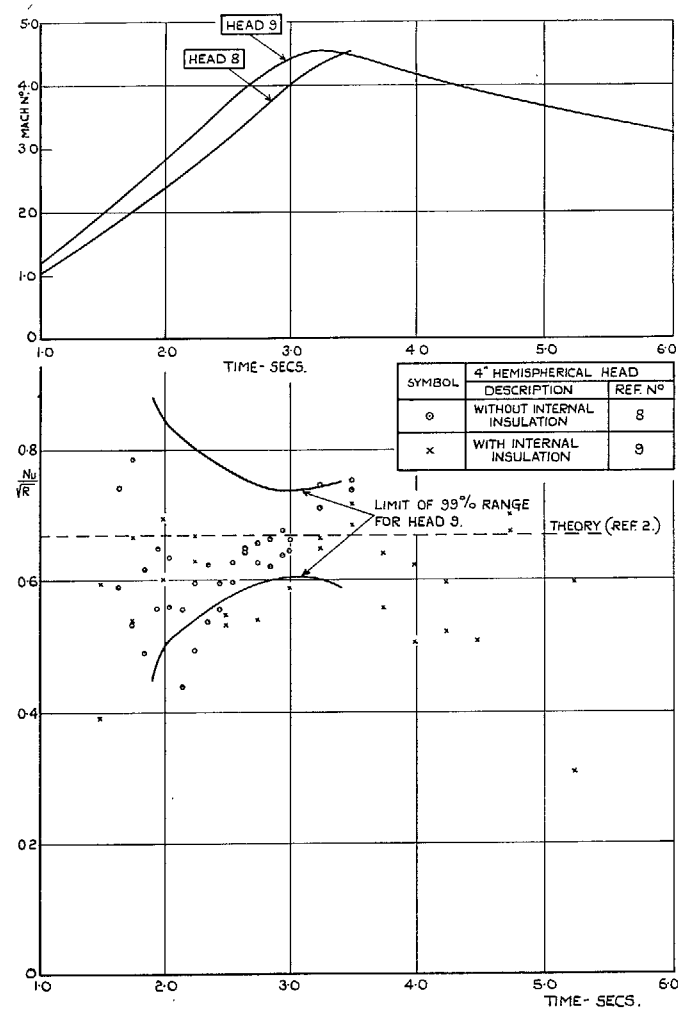


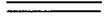



FIG. 26b. Variation of Nu/\sqrt{R} with time and Mach number for 4 in. hemispheres at stagnation point.


 LAMINAR FLOW THROUGHOUT RECORD

 TURBULENT FLOW THROUGHOUT RECORD

 RANGE OF ANGLES CONTAINING TRANSITION
 BOUNDARY FOR SOME PART OF RECORD

 THERMOCOUPLE POSITION.

FIGURES IN BRACKETS UNDER SOME ANGLES REFER
 TO RATIO BETWEEN MEASURED (THIS EXPERIMENT)
 AND THEORETICAL (LAMINAR FLOW-REF. 2)
 HEAT-TRANSFER RATES. SEE SECTION 6-3

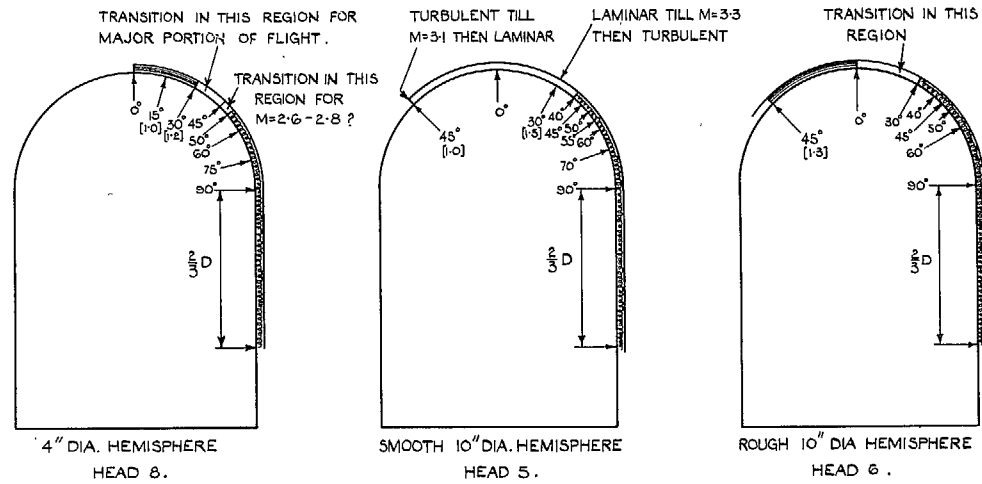


FIG. 27. Flow regimes on hemispherical heads.

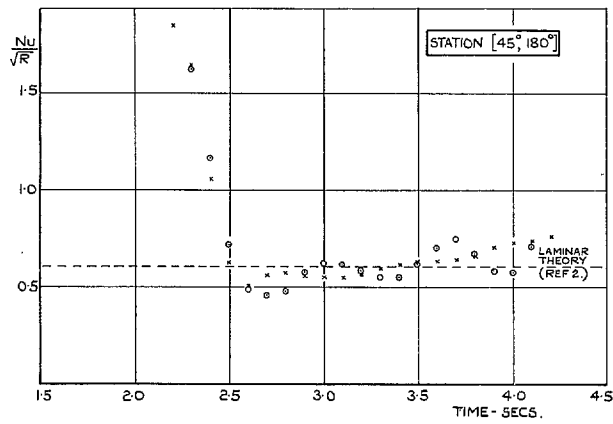
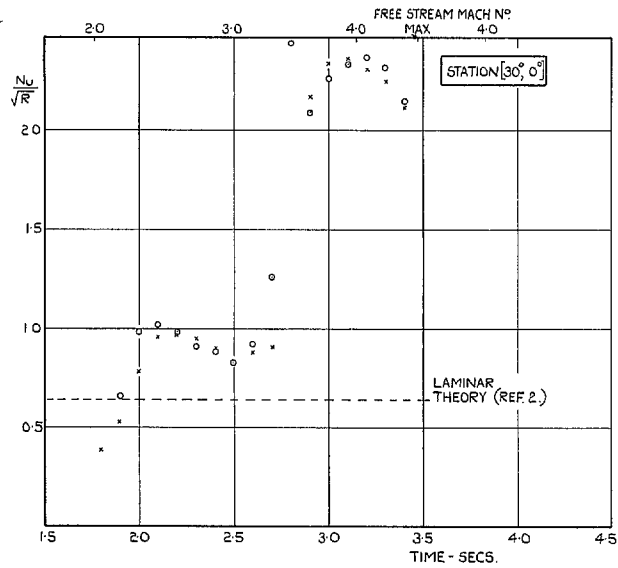


FIG. 28. Variation of Nu/\sqrt{R} with free-stream Mach number at stations $[30^\circ, 0^\circ]$ and $[45^\circ, 180^\circ]$ on smooth 10 in. hemisphere (head 5).

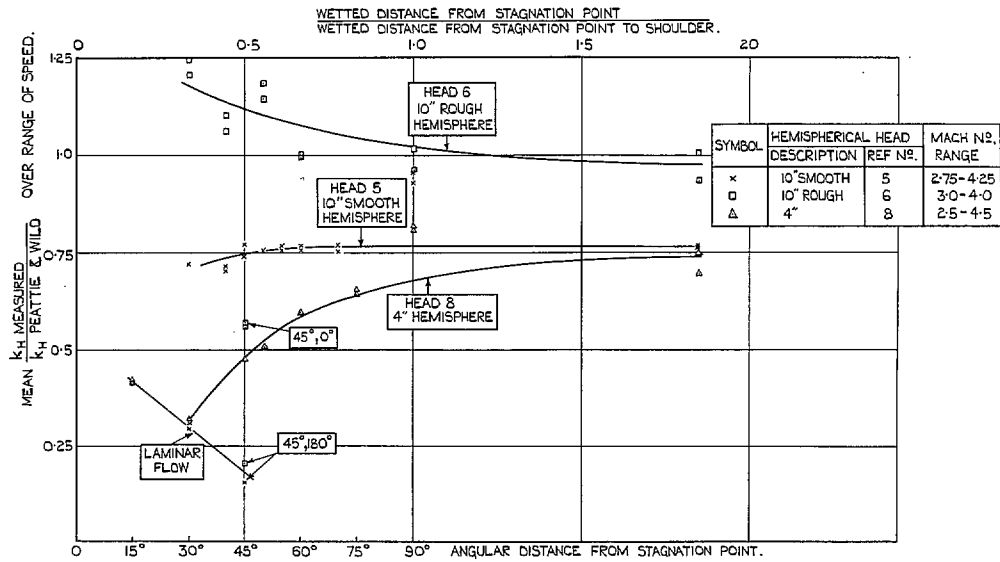


FIG. 29a. Comparison of measured heat transfer with that predicted by Peattie and Wild (Ref. 3) for hemispheres. Variation of mean value of ratio over Mach number range with angle.

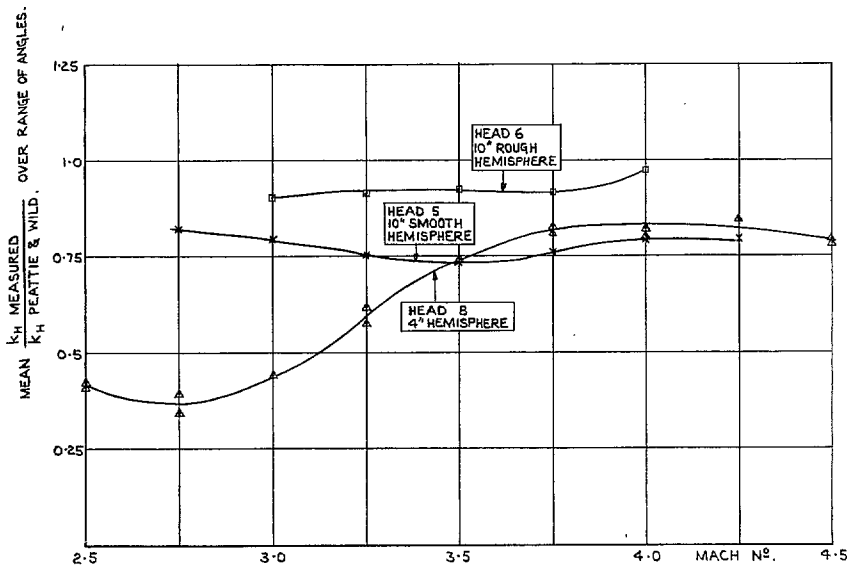


FIG. 29b. Comparison of measured heat transfer with that predicted by Peattie and Wild (Ref. 3) for turbulent flow round hemispheres. Variation of mean value of ratio over angle range with Mach number.

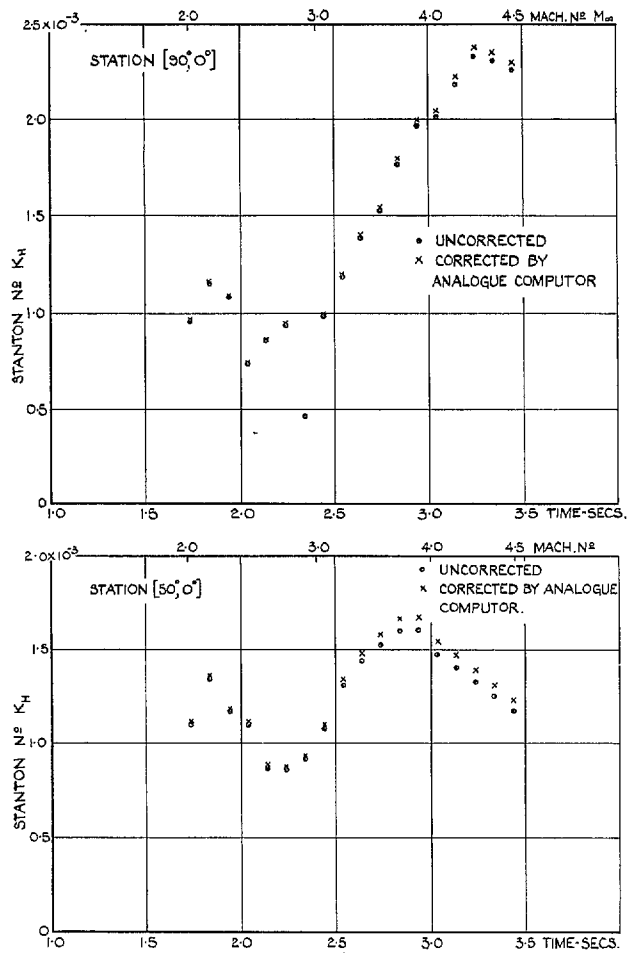


FIG. 30. Comparison of Stanton numbers, k_H , corrected and uncorrected for wall conductivity at two stations on the 4 in. hemisphere (head 8).

© *Crown copyright* 1967

Published by
HER MAJESTY'S STATIONERY OFFICE

To be purchased from
49 High Holborn, London w.c.1
423 Oxford Street, London w.1
13A Castle Street, Edinburgh 2
109 St. Mary Street, Cardiff
Brazennose Street, Manchester 2
50 Fairfax Street, Bristol 1
35 Smallbrook, Ringway, Birmingham 5
7-11 Linenhall Street, Belfast 2
or through any bookseller